Civil Engineering Graduate Theses & Dissertations   Civil, Environmental, and Architectural Engineering

Spring 1-1-2016

Enhancing Efficiency of Uv Advanced Oxidation Processes Via Iron Addition

Sydney L. Ulliman
University of Colorado at Boulder, Sydney.Ulliman@colorado.edu

Enhancing Efficiency of UV Advanced Oxidation Processes via Iron Addition

by

Sydney Ulliman

B.S., Civil Engineering, University of Gonzaga, 2011

A thesis submitted to the Faculty of the
Graduate School of the University of Colorado in partial fulfillment
of the requirement for the degree of
Master of Science
Department of Civil, Environmental and Architectural Engineering
2016

This thesis entitled:
Enhancing Efficiency of UV Advanced Oxidation Processes via Iron Addition
written by Sydney Ulliman
has been approved for the Department of Civil, Environmental and Architectural Engineering

Karl G. Linden, Ph.D

Chad J. Seidel, Ph.D

Fernando L. Rosario-Ortiz, Ph.D

Date

The final copy of this thesis has been examined by the signatories, and we
find that both the content and the form meet acceptable presentation standards
of scholarly work in the above mentioned discipline.

Abstract

Ulliman, Sydney (M.S., Environmental Engineering, Department of Civil, Environmental and Architectural Engineering)

Enhancing Efficiency of UV Advanced Oxidation Processes via Iron Addition

Thesis directed by Professor Karl G. Linden

Advanced oxidation processes (AOPs) have been recognized as a treatment technology to effectively remove a wide range of organic compounds in wastewater. Among different AOP methods, ultraviolet irradiation with hydrogen peroxide (UV/H_2O_2) is one of the leading technologies currently employed in numerous water treatment projects. Iron-assisted UV/H_2O_2, an alternative UV/AOP technology which uses photo-Fenton reactions (UV + H_2O_2 + iron) to increase hydroxyl radical production, has been used to effectively reduce organics at circumneutral pH; however, previous studies have evaluated iron-assisted UV/H_2O_2 systems using of high iron (>0.3 mg/L) and hydrogen peroxide concentrations (>10 mg/L) for wastewater treatment applications.

The goal of the present study was to evaluate the enhanced oxidation potential of iron-assisted UV/H_2O_2 using iron levels below USEPA secondary drinking water standards (0 to 0.3 mg/L). Chemically and kinetically diverse compounds para-chlorobenzoic acid (pCBA), carbamazepine (CBZ), and n-nitrosodimethylamine (NDMA) were selected to assess if low-levels of iron increased chemical degradation, and subsequently observe chemical-specific responses to iron-enhanced UV/H_2O_2 treatment. A quasi-collimated low-pressure UV device was used to expose low-carbon tap water (LCT) and well water samples to UV only, and samples dosed with 5 and 10 mg/L hydrogen peroxide and incremental ferrous and ferric iron levels typical of well waters. Steady-state hydroxyl radical (HO·) production was determined using radical probe pCBA. Degradation rate constants were experimentally determined for all test scenarios and compared against modeled results.

Iron-assisted UV/H_2O_2 efficiency at neutral pH was shown to be most influenced by photochemical and kinetic properties of the target chemical and the water matrix. Contrary to previous studies using higher levels of iron and H_2O_2 (>10 mg/L), chemical removal rates were not impacted by iron species, iron concentration or H_2O_2 concentration. With the exception of NDMA, chemical degradation was not improved in LCT water for iron-assisted UV/H_2O_2

scenarios presumably due to the absence of organic and inorganic ligands. For iron-assisted UV/H_2O_2 tests conducted in well water, a 20% increase in $HO^{\cdot}$ production was observed as measured by the radical probe pCBA, and NDMA degradation rates increased by 14% to 24%. CBZ removal was neither improved or inhibited by the presence of iron. Interestingly, NDMA was the only chemical where iron addition increased removal rates in LCT and well water. Furthermore, iron without H_2O_2 addition was shown to enhance NDMA removal by 38% in LCT water and 8% in well water when compared to UV photolysis alone.

This work provides an understanding of the fundamental role of iron in a UV/H_2O_2 systems, provides a basis for improved modeling of AOPs in the presence of iron, and could indicate a strategy for improving the efficiency of UV/AOP treatment.

Dedication

This thesis is dedicated first to my parents, Nancy and Curt, whom, from the time I was small, told me I could achieve anything to which I set my mind; they gave me the confidence to jump without fear of falling. To my academic role-models at Gonzaga University, Professors Mara London and Susan Norwood, for showing me the importance of water treatment on both an engineering and humanitarian level. Finally, to my partner Alan, for his patience, encouragement, and support through the rollercoaster rides of life.

Acknowledgements

First and foremost, I would like to acknowledge my advisor, Prof. Karl Linden, for patiently guiding me through my first research project. As a result of his support, I have become a stronger student and researcher, and I know under his continued supervision I will continue to grow in both these areas. To my committee members, Dr. Chad Siedel and Prof. Fernando Rosario-Ortiz, thank you for taking the time to review my thesis and provide valuable feedback.

I greatly appreciate the chemistry help provided by Prof. Fernando Rosario-Ortiz and Prof. Joseph Ryan. I would like to thank Steffen Graham him for his time and efforts on this research project. To the Linden lab team, thank you for making my experience at the University of Colorado wonderful and motivating me daily.

Finally, I would sincerely like to thank Garrett McKay for his encouragement, invaluable analytical support, and research ideas throughout this project.

Table of Contents

List of Tables

List of Figures

Introduction

UV-based advanced oxidation processes (UV/AOPs) combine UV light with hydrogen peroxide, or other oxidizers, to simultaneously photolyze and oxidize micropollutants in water supplies (Swaim et al., 2008; Oppenlander, 2002). While highly effective at removing many pollutants, the water matrix treated by UV/AOPs can greatly impact removal efficiency. Carbonate species, dissolved organic carbon (DOC), and nitrite ions are known to inhibit hydroxyl radical (HO˙) reactions with target pollutants through a process known as scavenging (Rosenfeldt and Linden, 2007). Light screening by the water matrix can also impact performance by decreasing the UV light intensity, thereby preventing both direct photolysis and photolysis of the added oxidizer. Iron is a water quality parameter commonly associated with inhibiting UV light intensity by increasing the absorbance of the water. Furthermore, the presence of iron in potable water is not desirable. Although not toxic, oxidized iron can cause staining of household items, and taste and odor issues. For these reason the Environmental Protection Agency (EPA) recommends a Secondary Maximum Contaminant Limit (MCL) of 0.3 mg/L total iron. UV system manufacturers also require iron levels less than 0.3 mg/L to prevent quartz sleeve fouling which can result in decreased UV intensity

Although seemingly desirable to remove iron prior to UV/AOPs, iron in the presence of light and hydrogen peroxide has been shown to increase the net production of oxidizing species in UV/AOPs utilizing hydrogen peroxide (UV/H_2O_2) through Fenton and photo-Fenton reactions (Pignatello et al., 2006; Rahim Pouran et al., 2015). Similar to UV/AOPs, the primary oxidant produced and responsible for chemical transformation in the Fenton reaction is the highly reactive, non-selective hydroxyl radical (HO·), generated via pathway 1:

$$Fe^{2+} + H_2O_2 \rightarrow Fe^{3+} + HO^- + HO^˙ \ (1)$$
$$Fe^{3+} + H_2O_2 \rightarrow Fe^{2+} + HO_2^˙ + H^+ \ (2)$$
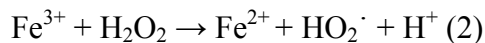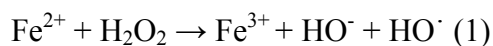
Under acidic (pH<3) conditions in the absence of organics, soluble ferrous, Fe(II), and ferric iron, Fe(III), are cycled autocatalytically to produce HO·, reaction 2. Photoassisted Fenton (photo-Fenton) reactions, where ferric iron is photoreduced to ferrous iron in the presence of

light, have been shown to enhance chemical removal rates compared to dark-Fenton reactions (Pignatello et al., 2006). This is due to increased generation of HO· directly by H_2O_2 photolysis (3) and indirectly from regenerating Fe(II) (4) when Fe(III) undergoes photoreduction to Fe(II) via ligand-to-metal charge transfer (LMCT).

$H_2O_2 + hv \rightarrow 2HO^{·}$ (3)

$Fe^{3+}(L)_n + hv \rightarrow Fe^{2+}(L)_{n-1} + L^{·}$ (4)
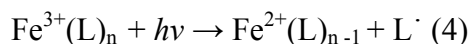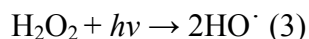
While commonly viewed as an economical and relatively easy treatment option for micropollutant removal, photo-Fenton applications have been limited to non-potable water treatment due to the need for acidification to prevent Fe(III) and Fe(II) precipitation. Subsequent neutralization can result in iron sludge production and added costs for sludge disposal. Researchers (Chong et al., 2010; Teel et al., 2001; Doumic et al., 2015) have explored using heterogeneous and homogeneous catalysts to stabilize Fe^{3+} at neutral pH, however, use of catalysts have several disadvantages including removing or re-generating the catalyst, a potential increase in toxicity, and overall increased costs (Rahim Pouran et al., 2015; Sun and Pignatello, 1992).

Several studies (Klamerth et al.; 2010; Ortega-Gómez et al., 2016; Vermilyea and Voelker, 2009; Bernabeu et al., 2012; Southworth and Voelker, 2003; Rubio et al., 2013; De la Cruz et al., 2012, 2013; Vione et al., 2014a; Neamţu et al., 2014; Velo-Gala et al. 2014; Pérez et al., 2002) have successfully demonstrated photo-Fenton reactions to degrade micropollutants without catalyst addition or acidification. Fenton and photo-Fenton reactivity decreases as pH increases above 3 due to Fe(III) precipitation via hydrolysis and subsequent formation of unstable aquo-Fe(III) complexes. Figure 1 illustrates iron speciation with respect to pH. However, in the presence of dissolved organic matter (DOM) Fe(III) can form a more stable complexes with organic ligands. These complexes are also more reactive when compared to aquo-Fe(III) complexes since they have higher molar absorption coefficients and quantum yields (Southworth and Voelker, 2003; King and Farlow, 2000; Aldrich et al., 2001) .
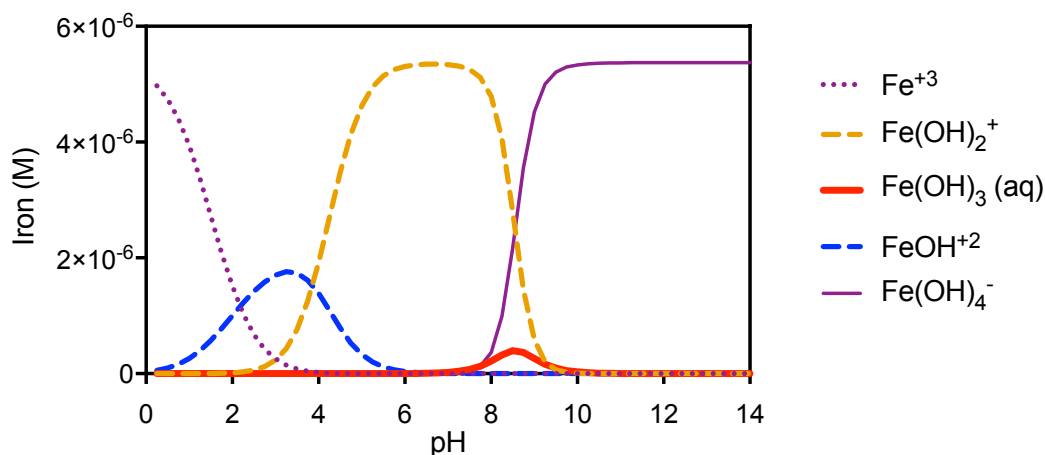
Figure 1. Iron speciation diagram with respect to pH. Generated using Visual Minteq program.

A few studies have used UV_{254n} as a light source (De la Cruz et al., 2012, De la Cruz et al., 2013, Neamțu et al., 2014; Velo-Gala et al., 2014) to evaluate photo-Fenton parameters under neutral pH conditions. With the exception of Velo-Gala et al., iron levels far exceed the 0.3 mg/L total iron limit recommended by the EPA and, for all studies, H_2O_2 levels exceed concentrations typical of conventional UV/H_2O_2 systems which are between 3 and 10 mg/L (Swaim et al., 2008). Broadly, the impetus for these studies was to quantify photo-Fenton efficacy through organics reduction in wastewater. However, the reactivity of iron-assisted UV/H_2O_2 at neutral pH using low-levels of iron (< 0.3 mg/L) and hydrogen peroxide (<10 mg/L) is not well understood especially for drinking water applications. Furthermore, whether or not optimized photo-Fenton parameters, mainly iron to H_2O_2 molar ratios and iron species, are chemical-specific is unclear within the literature.

The present study investigates the enhanced oxidation potential of iron-assisted UV/H_2O_2 at neutral pH using low-levels of iron commonly present in well water. To assess chemical-specific responses to photo-Fenton reactions, kinetically diverse compounds para-chlorobenozoic acid (pCBA), carbamazepine (CBZ) and n-nitrosodimethylamine (NDMA) were exposed to UV_{254} under varied Fe(II) and Fe(III) concentrations (0- 0.3 mg/L) and H_2O_2 concentrations (0-10 mg/L). Experiments were conducted in low-carbon tap water (LCT) and well water to evaluate the role of organic compounds in photo-Fenton reactions. pCBA was used as an HO˙ probe to determine steady-state HO˙ production for UV/H_2O_2 systems with and without iron. Degradation rate constants were experimentally determined for all test scenarios and theoretical degradation rates were determined using a model.

Methods and Materials

Experimental plan

Bench-scale experiments were conducted to test the degradation of selected chemicals under UV/H_2O_2 with and without iron. Tests were performed in low-carbon tap water and well water using 0, 0.1, 0.3 mg/L Fe(II) and Fe(III) iron and 0, 5, 10 mg/L H_2O_2. The test matrix can be viewed in Appendix B.

Reagents and test waters

Analytical grade chemicals para-chlorobenozoic acid, carbamazepine and *n*-nitrosodimethylamine and were purchased from Sigma-Aldrich (>98%). All stock solutions, chemicals, hydrogen peroxide (BDH), sodium thiosulfate (Sigma-Aldrich), ferrous sulfate heptahydrate (Fluka Chemika) and ferric chloride (Fisher Scientific), were prepared in ultrapure water (resistance = 18 MΩ cm). 1,10 phenanthroline reagent powder packets for total and ferrous iron determination were purchased from HACH (Loveland, Colorado). Low carbon tap water, tap water filtered through activated carbon for organics and chlorine removal, and raw well water from Minneapolis, MN, served as water sources for exposure experiments; Table 1 shows the basic water quality data for both sources. Samples were stored at 4°C.

Table 1. Water quality for low-carbon tap (LCT) water and well water.

Parameter	LCT water	Well water
TOC (mg-C/L)	0.25	0.72
Alkalinity (mg/L as $CaCO_3$)	42	270
Nitrate (mg-N/L)[*]	ND	ND
Nitrite (mg-N/L)[*]	ND	ND
UV 254nm (cm^{-1})	LDL[**]	1.15E-02
pH	6.72	7.78

[*]Detection limit of 0.015 mg/L-N
[**]LDL is lower detection limit

Sample Preparation

For each experiment, the various constituents were added to the test water in a specific order: micropollutant, iron, hydrogen peroxide addition was maintained throughout experiments. Solutions were spiked with the target chemical at a concentration equal to 100x the high

performance liquid chromatography (HPLC) instrument detection limit, resulting in starting concentrations of 0.5 mg/L for NDMA and pCBA, and 1.0 mg/L for CBZ. Iron stock solutions were prepared daily at 10 to 15 mg/L Fe concentrations to achieve freshly precipitated colloidal iron oxyhydroxides and added into the experimental matrix to achieve 0.1 and 0.3 mg/L Fe^{2+} and Fe^{3+} concentrations. Stock and sample iron concentrations were measured using 1, 10 phenanthroline reagent powder packets then later confirmed with inductively coupled plasma optical emission spectrometry (ICP-OES). Samples for ICP-OES analysis were acidified with nitric acid (pH<2) for preservation. Hydrogen peroxide was added to attain 5 mg/L and 10 mg/L concentrations (Klassen et al., 1994) within minutes of the UV exposures. Residual hydrogen peroxide was quenched with 10mg/L sodium thiosulfate and pCBA and NDMA samples were filtered with 0.45 μm nylon filter (VWR). Because of interferences with the nylon filter, CBZ was filtered with a 0.2 μm Acrodisc Supor ® membrane filter for particulate removal prior to HPLC analysis.

UV Irradiation Experiments

A bench-scale collimated dual-beam low-pressure UV device was used for sample exposure. Four low-pressure UV (LPUV) lamps (15 watt, #G15T8) were housed above two 4-inch apertures, each equipped with a manual shutter. Incident UV irradiance at 254 nm was measured by a calibrated radiometer and detector (International Light Inc., Model 1700/SED 240/W). UV fluence was calculated by multiplying the average irradiance by the exposure time in seconds. The average irradiance was determined by correcting the incident irradiance for sample depth, absorbance at 254 nm, surface reflectance, and petri factor (Bolton and Linden 2003). Samples were taken at fluence rates ranging from 0 to 1000 mJ/cm^2. All glassware was acid washed and scrubbed between experiments to remove residual iron.

Control Experiments

Several control experiments were performed to understand if 1) iron was complexing with target chemicals, 2) dark Fenton reactions were contributing to chemical degradation, 3) loss of iron was occurring and 4) water quality parameters, mainly pH and temperature, were changing during dark and photo-Fenton experiments.

To determine if iron was complexing with the target chemical resulting in physical removal after filtration, UV exposed samples containing iron were acidified (pH<2) using hypochlorous acid, HPLC analyzed, and then results were compared to unacidified filtered

5

samples (Appendix F). Peak areas between the acidified and unacidified filtered samples varied by ±8% for all three chemicals (Appendix E) indicating iron was not complexing with the chemical and being removed by filtration. Dark experiments were performed in a light impenetrable reactor. The contribution of dark Fenton reactions to chemical degradation were shown to be negligible (Appendix G). This may be attributed to the short time period (<20 minutes) the samples were allowed to mix. To verify that iron stayed suspended in solution and did not absorb to the quartz vessel, iron concentrations prior to and after UV and dark experiments were determined via ICP-OES. As shown in Appendix D, minor (3%) iron loss did occur in some scenarios during UV and dark experiments. In addition to controlling iron, temperature and pH were also monitored (Appendix E). Up to a 4°C temperature change occurred after exposing a 75 mL sample for the maximum UV fluence rate (~ 18 minutes). Change in pH from pre to post-irradiated samples was minimal (± 0.3 pH units).

Analysis

An Agilent 1100 series high performance liquid chromatograph equipped with a UV detector and a reverse phase C-18 column was used to analyze chemical concentrations. pCBA was eluted with 10 mM phosphate: methanol (v:v=45:55) using 234nm for detection; the mobile phase for CBZ consisted of acetonitrile: ultrapure water (v:v=40:60), 286nm for detection; the elution process for NDMA was methanol: 25 mM phosphate buffer at pH 6.5, 230nm for detection. All sample methods used a 1 mL/min flowrate. Iron stock solution concentrations were measured with 1,10 phenanthroline reagent powder packets. A set of control tests were conducted to verify 1,10 phenanthroline measurements aligned with ICP-OES measurements (Appendix D). Prior to ICP-OES analysis, samples were acidified with nitric acid.
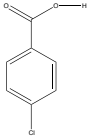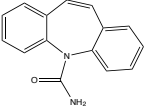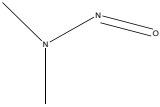
Results and Discussion

Chemical Selection

Compounds *N*-Nitrosodimethlyamine (NDMA) and Carbamazepine (CBZ) were selected based on their photochemical and physicochemical properties. para-Chlorobenzoic acid (pCBA), a common HO˙ probe with well-established kinetic values, and CBZ were used as controls to

monitor radical activity in UV/H_2O_2 and photo-Fenton experiments. Relevant chemical properties of each compound are shown in Table 2.

Table 2. Pertinent photochemical and physiochemical properties of selected compounds. Kinetic data taken from Buxton et al., 1988; Wols and Hofman-Caris, 2012; Sharpless and Linden, 2003.

Chemical units	k_{HO} $M^{-1}s^{-1}$ (10^9) $M^{-1}s^{-1}$	Φ_{254} (10^{-2}) mol Einstein^{-1}	ε_{254} (10^3) $M^{-1}cm^{-1}$	Molecular Weight g mol^{-1}	Solubility in Water, 25 °C mg L^{-1}
para-chlorobenzoic acid (pCBA)	5.00	1.3	2.37	156.6	77
carbamazepine (CBZ)	8.02 (±1.90)	0.06	6.07	236.3	125
N-nitrosodimethylamine (NDMA)	0.380 (±0.071)	24.8 (±10.2)	1.65	74.1	Infinitely soluble

Average quantum yield values for CBZ and pCBA are respectively 214 and 19 times lower than NDMA's quantum yield, whereas second order HO˙ rate constant (k_{HO}) are 21 and 13 times higher. Therefore, it can be concluded that CBZ and pCBA removal by HO˙ oxidation is far more effective than direct photolysis. Low-pressure UV irradiation alone cannot degrade CBZ due to its low quantum yield (Keen et al., 2012). In contrast, NDMA, with a relatively high quantum yield, low second order HO˙ rate constant and strong absorption spectra from 200-275nm, degrades mainly through photolysis. Illustrated in Figure 2 are the diverse molar absorption spectra for all three chemicals, hydrogen peroxide and Fe(II) and Fe(III).
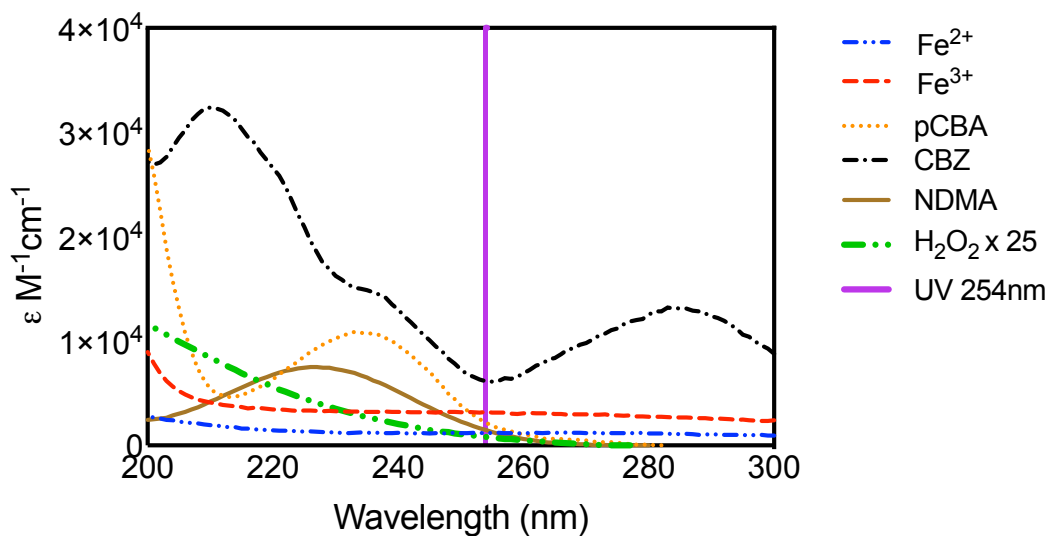
Figure 2. Molar absorption spectra of selected chemicals, iron, and hydrogen peroxide from 200 to 300nm.

Radical Determination

To compare and assess radical reactivity for UV/H_2O_2 and UV/ H_2O_2 iron assisted experiments, steady-state HO˙ concentrations were determined using pCBA and CBZ as HO˙ probes. (HO˙ calculations are provided in Appendix H.) UV/H_2O_2 driven HO˙ steady-state values (Table 3) calculated using pCBA and CBZ in well water are within ± 0.15M of each other whereas LCT are ± 2.67.

Table 3. Steady-state UV/H_2O_2 hydroxyl radical concentrations determined for pCBA and CBZ for LCT and well water.

Chemical	Experiment	LCT Average [OH] (M) x 10^{-13}	Well Average [OH] (M) x 10^{-13}
pCBA	5mg/L H_2O_2	5.872	1.095
	10mg/L H_2O_2	8.410	2.145
CBZ	5mg/L H_2O_2	3.012	1.237
	10mg/L H_2O_2	5.936	2.509

Second order hydroxyl radical reaction rate constants, $k_{HO˙}$, were taken from the literature and used to determine HO˙ steady-state concentrations (values provided in Appendix H). While the $k_{HO˙}$ value for pCBA is well-accepted, CBZ $k_{HO˙}$ values vary within the literature. A competition kinetic experiment could be performed to determine the $k_{HO˙}$ for CBZ this specific system.

Illustrated in Figure 3 are the HO˙ steady-state concentrations for pCBA and CBZ in well water (results for LCT water not shown). All pCBA test scenarios show increased HO˙ production after iron addition whereas increased HO˙ in CBZ is observed only for Fe(II) and 5 mg/L H_2O_2 scenarios.
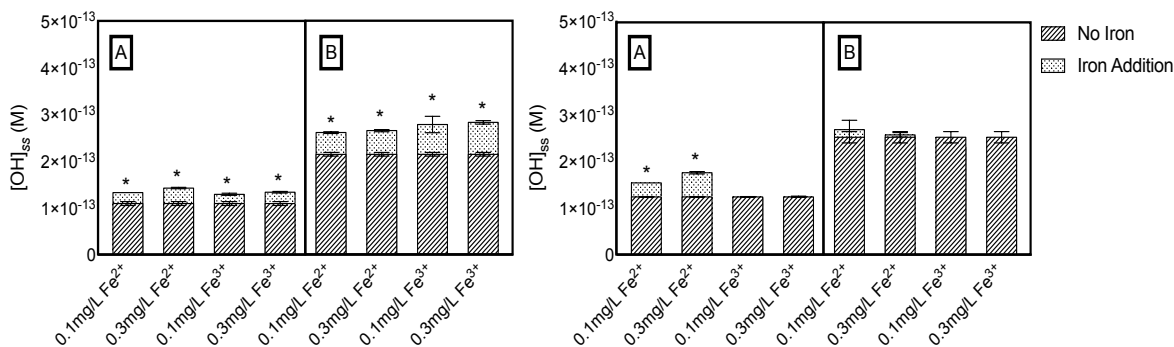
Figure 3. Steady-state hydroxyl radical production determined for pCBA (left) and CBZ (right) with 5 mg/L H_2O_2 (A) and 10 mg/L H_2O_2 (B) in well water. Error bars represent the standard deviations between duplicate experiments and (*) denotes 95% confidence in the difference between iron addition and no iron results.

For this study, where $[H_2O_2] >> [Fe]$ and UV_{254nm} wavelength was used, HO˙ is assumed to be the reactive species responsible for chemical degradation. It is worth noting that HO˙ is most likely not the only radical species present in photo-Fenton systems. Radical species identified in Fenton and other AOPs are the peroxyl radical (ROO˙), the hydroperoxyl radical (HO$_2$˙) and its conjugated base, the superoxide anion ($O_2^{-˙}$) (Pignatello et al., 2006). Reactive species unique to Fenton reactions are iron-oxo species, mainly the ferryl ion, FeO_2^+ (Keenan and Sedlak, 2008, Minero et al., 2013, Bauer and Fallmann, 1997, Mártire et al., 2002, (Vione et al., 2014b). HO˙ and ferryl are said to be produced concurrently in Fenton reactions and utilize similar mechanisms (electron transfer) for chemical degradation. For dark-Fenton reactions at neutral pH in natural systems, Miero et al. and (Vione et al., 2014a) gave evidence that the concentration of ferryl to HO˙ was 60:40. For photo-Fenton systems where H_2O_2 is in excess and being rapidly photolized by a high intensity light source, the concentration of ferryl is minimal compared to HO˙. In addition, ferryl's second order reaction rate constants determined by Bautz et al. for nitrophenols were approximately five orders of magnitude lower than HO˙ (Bautz et al., 2006). More information on ferryl is provided in Appendix A under Radical Species Present in Fenton Reactions.

With the exception of Fe(II) and 5 mg/L H_2O_2 CBZ test scenarios, HO˙ production showed no dependence on iron species. Whether or not Fe(II) iron enhances HO˙ production over Fe(III) is debated within the literature. Without the presence of organics in acidic conditions, the initial iron species is argued not to matter when H_2O_2 is in excess since Fe (III) will quickly reduce to Fe(II) and Fe(II) will oxidize to Fe(III) (Pignatello et al., 2006). However, Gallard and Laat found Fe(II) addition can result in a greater HO˙ production due to the fast reaction between Fe(II) and H_2O_2 when compared to the slow reaction of Fe(III) with H_2O_2 (2) (Gallard and De Laat, 2000, Chen and Pignatello, 1997). This could partially explain why CBZ removal rates were higher with ferrous iron with 5 mg/L of H_2O_2, however, similar trends would be expected for 10 mg/L H_2O_2 scenarios.

In theory, the net HO˙ production should be the same for all pCBA and CBZ scenarios with and without iron addition. The results shown in Figure 6 coupled with the evidence provided against transient oxidants, other than HO˙, contributing to chemical removal indicate chemical-specific interactions with iron. For example, the electron-poor carboxylate group on pCBA could complex to Fe(III) resulting in photooxidation through LMCT. Whereas for CBZ, steric repulsion from its three fused rings might prevent iron complexation.

Degradation kinetics of selected compounds

Degradation kinetics were experimentally determined to observe the influence varied H_2O_2 concentration, iron species and concentration had on chemical removal rates for UV/H_2O_2 systems. The degradation of pCBA, CBZ, and NDMA is represented by the pseudo first-order rate constants, *k'$_{obs}$,* which can be determined by plotting equation 1 and determining the slope (*k'$_{obs}$*).

$$Ln\left(\frac{[C]}{[C_o]}\right) = -k'_{obs} * F \qquad (1)$$

Where *Ln([C]/[C$_o$])* is the natural log of the ratio of chemical concentration at a given fluence over the initial chemical concentration and *F* is the UV fluence (mJ/cm^2). Degradation rate constants with corresponding data set confidence intervals are provided in Appendix I.

Fluence-based units were chosen to reflect changes in experimental conditions and provide a comparative unit for future UV-based iron-assisted AOP. Pseudo first-order kinetics

were observed for all experiments. Graphical results are presented in Figure 4 and tabulated results in Table 4.

Figure 4. Pseudo first-order reaction rate constants for LCT water (A) and well water (B) for UV/H_2O_2 and iron-catalyzed UV/H_2O_2. Dashed line separates experiments with and without iron addition.
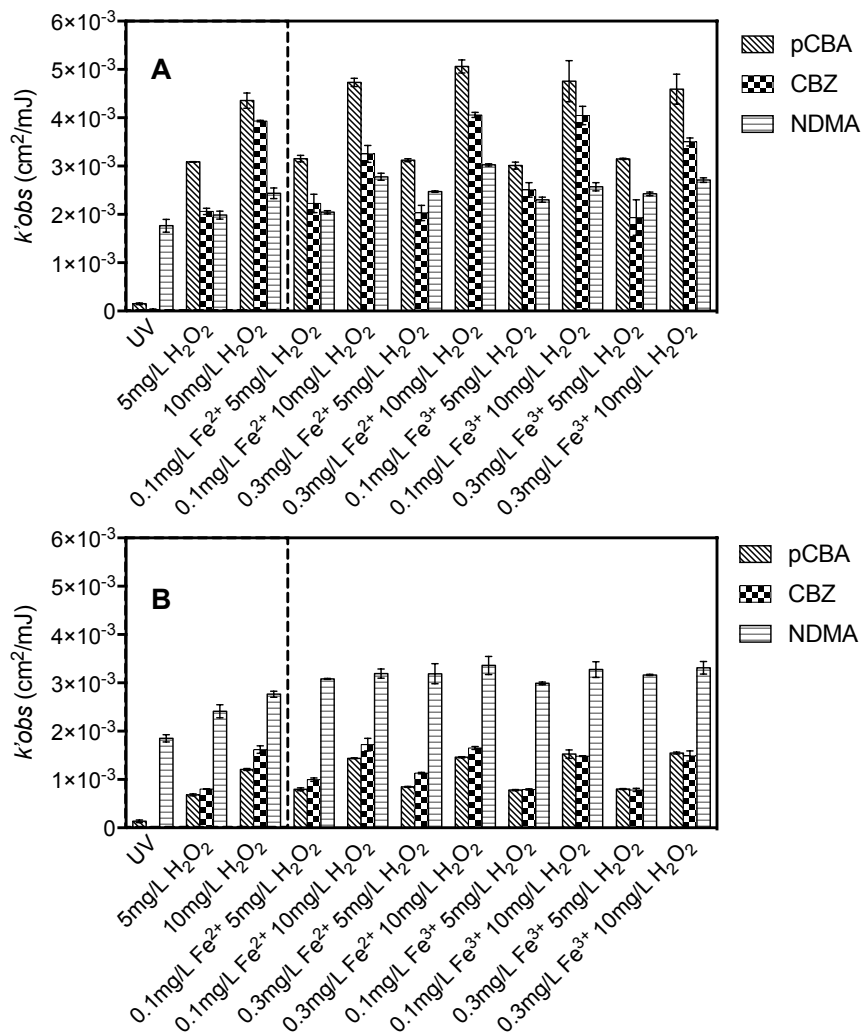
Table 4. Corresponding pseudo first-order reaction rate values for Figure 4.

		LCT Water		
		pCBA	CBZ	NDMA
Experiment		Average k'_{obs} (cm^2/mJ)		
UV		1.506E-04	2.510E-05	1.763E-03

11

5mg/L H_2O_2	3.087E-03	2.063E-03	1.985E-03
0.1mg/L Fe^{2+} 5mg/L H_2O_2	3.155E-03	2.225E-03	2.043E-03
0.3mg/L Fe^{2+} 5mg/L H_2O_2	3.123E-03	2.030E-03	2.474E-03
0.1mg/L Fe^{3+} 5mg/L H_2O_2	3.012E-03	2.509E-03	2.303E-03
0.3mg/L Fe^{3+} 5mg/L H_2O_2	3.148E-03	1.934E-03	2.426E-03
10mg/L H_2O_2	4.356E-03	3.934E-03	2.501E-03
0.1mg/L Fe^{2+} 10mg/L H_2O_2	4.731E-03	3.254E-03	2.780E-03
0.3mg/L Fe^{2+} 10mg/L H_2O_2	5.063E-03	4.058E-03	3.027E-03
0.1mg/L Fe^{3+} 10mg/L H_2O_2	4.757E-03	4.048E-03	2.572E-03
0.3mg/L Fe^{3+} 10mg/L H_2O_2	4.592E-03	3.501E-03	2.711E-03

	Well water		
	pCBA	CBZ	NDMA
Experiment	Average k'_{obs} (cm^2/mJ)		
UV	1.351E-04	1.285E-05	1.853E-03
5mg/L H_2O_2	6.827E-04	8.046E-04	2.414E-03
0.1mg/L Fe^{2+} 5mg/L H_2O_2	7.983E-04	9.967E-04	3.082E-03
0.3mg/L Fe^{2+} 5mg/L H_2O_2	8.475E-04	1.134E-03	3.082E-03
0.1mg/L Fe^{3+} 5mg/L H_2O_2	7.809E-04	7.939E-04	2.990E-03
0.3mg/L Fe^{3+} 5mg/L H_2O_2	8.029E-04	7.847E-04	3.163E-03
10mg/L H_2O_2	1.208E-03	1.618E-03	2.765E-03
0.1mg/L Fe^{2+} 10mg/L H_2O_2	1.440E-03	1.723E-03	3.192E-03
0.3mg/L Fe^{2+} 10mg/L H_2O_2	1.460E-03	1.653E-03	3.361E-03
0.1mg/L Fe^{3+} 10mg/L H_2O_2	1.527E-03	1.483E-03	3.276E-03
0.3mg/L Fe^{3+} 10mg/L H_2O_2	1.549E-03	1.489E-03	3.312E-03

pCBA and CBZ low-carbon tap (LCT) water decay rates were on average 72% and 57% higher over those in well water due to increased concentrations of ˙OH scavengers, mainly carbonate species and dissolved organic matter (DOM), present in the well water (Table 1). Unexpectedly, NDMA degradation rate constants increased between 30% to 40% in well water when compared to LCT water. Presented in Figure 5 are side-by-side LCT and well water reaction rates.
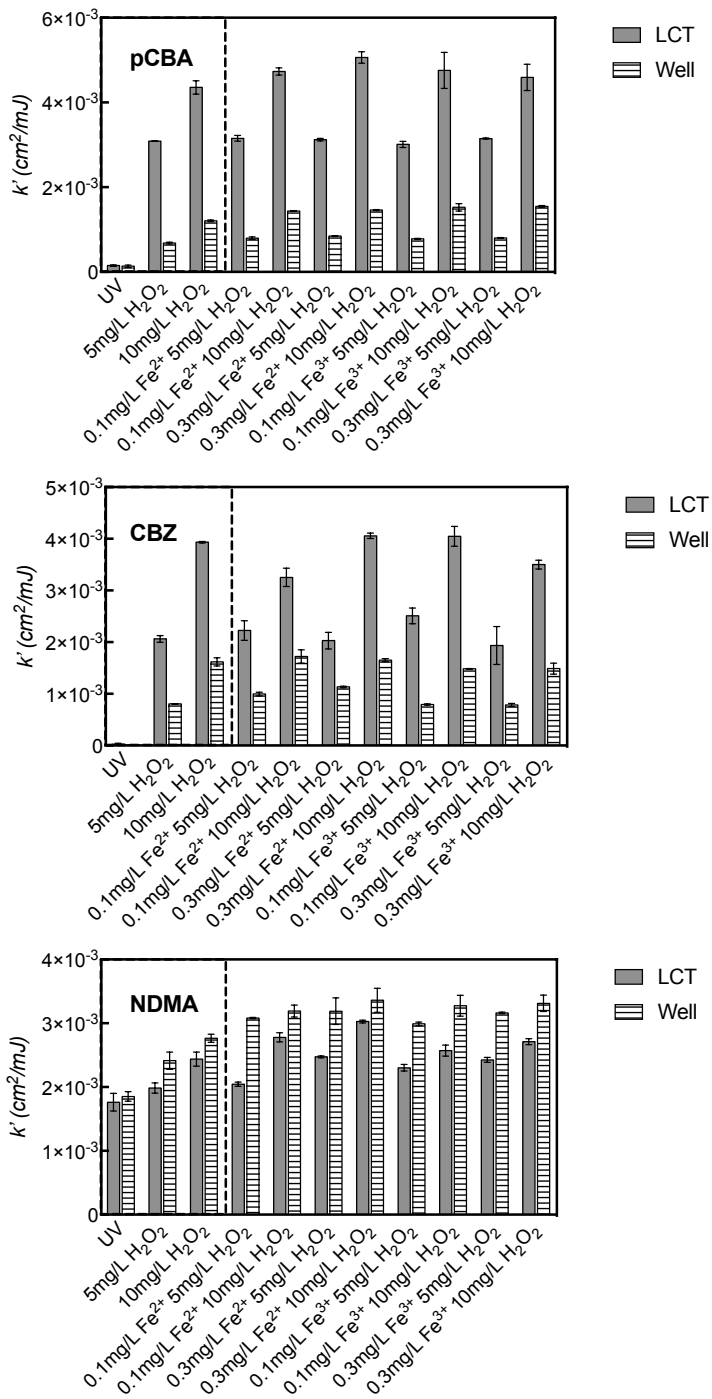
Figure 5. pCBA, CBZ and NDMA pseudo-first-order reaction rate constants for LCT and well water. Error bars represent the standard deviations between duplicate experiments.

Low-level iron addition was shown to increase pCBA and NDMA degradation rates for all iron-assisted UV/H$_2$O$_2$ tests in well water by 14%-22% and 13%-24%, respectively, whereas CBZ removal was neither improved nor inhibited. Statistically, chemical removal in the LCT water was not improved with iron addition for either chemical (p > 0.05). This can be explained by the stable iron complexes formed with organic ligands when Fe(III) undergoes photoassisted LMCT in well water. For this study, the iron complex formed was most likely Fe(CO$_3$) since relatively high alkalinity (270 mg/L as CaCO$_3$) was present in the well water. King and Farlow and Aldrich et al. showed dark-Fenton reactions in natural systems at pH 5 and above were increased in the presence of carbonate due the formation of the kinetically active Fe(CO$_3$) complex. These complexes also have higher quantum yields and molar absorption coefficients at UV$_{254}$ when compared to visible light resulting in a more reactive iron species (Pignatello et al., 2006). For the LCT water, containing six times less carbonate species than the well water, unstable and less reactive aquo-Fe(II) and Fe(III) complexes were likely present.

Molar ratio of hydrogen peroxide to iron concentration, [H2O2]:[Fe], is a parameter commonly evaluated in Fenton studies (Rahim Pouran et al., 2015, Pignatello et al., 2006). In photo-Fenton studies at neutral pH optimal organics removal has been achieved using [H$_2$O$_2$]:[Fe] ratios of 10:1 to 40:1 (Neamţu et al., 2014, Pérez et al., 2002). Degradation rate constants for all chemicals (Figure 6) showed no relationship to [H$_2$O$_2$]:[Fe] or iron concentration. Given the low-levels of iron used in this study, the fraction of iron able to participate in Fenton reactions, or potentially complex with the target compound, was most likely controlled by stable iron complexes formed.

Modeled Degradation Rates

All results were modeled using equation 1, following methods outlined by Sharpless and Linden, to compare predicted and experimental degradation rate constants of UV/H$_2$O$_2$ to iron-assisted UV/H$_2$O$_2$. Two parameters commonly used in photo-Fenton models are: a shield factor, to account for iron blocking H$_2$O$_2$ photolysis, and, in addition to photolysis and oxidant reaction rates, a third rate constant which considers Fenton reactivity, *k'$_{Fenton}$*. The model takes into consideration shielding effects from iron by incorporating the absorbance of the water sample. For the purposes of this study, the developed model was used as a tool for comparison, not for

prediction and, as such, the contribution of k'_{Fenton} was not incorporated. Appendix J provides model inputs and an example of modeled data.

$$\frac{d[C]}{dt} = k'_{model} = -(k'_d + k'_i)[C] \quad (1)$$

For equation 1, k'_d and k'_i (cm^2/mJ) represent the pseudo-first order rate constants for direct and indirect photolysis, respectively, multiplied by the chemical concentration, *[C]*. The determination of k'_i is shown in equations 2 and 3:

$$-\frac{d[C]}{dt} = k'_i[C] = k_{OH}[\bullet OH]_{ss}[C] \quad (2)$$

$$[\bullet OH]_{ss} = \frac{k_{a,H_2O_2}\Phi_{H_2O_2}[H_2O_2]}{\sum k'_s[S]} \quad (3)$$

Second order hydroxyl radical reaction rate constant, k_{OH} (M^{-1}s^{-1}), values taken from literature is multiplied by the steady-state HO$^{\cdot}$ and chemical concentration. Steady-state HO$^{\cdot}$ concentration (M) can then be calculated using (. Here, the denominator accounts for HO$^{\cdot}$ scavengers present in source waters by multiplying known second-order scavenger reaction rate constants, k'_s (M^{-1}s^{-1}), by the scavenger concentration (M). Scavenger rate constants and concentrations used for dechlorinated tap and well water are provided in Appendix J. The numerator is the HO$^{\cdot}$ production determined by multiplying $k_{a,H2O2}$ (Es mol^{-1}sec^{-1}), the specific rate of light absorbed by H$_2$O$_2$, by the molar concentration of H$_2$O$_2$ and quantum yield , $\Phi_{H_2O_2}$, (mol/Einstein) of H$_2$O$_2$. The specific rate of light absorption by H$_2$O$_2$ is calculated using equation 4.

$$k_{a,H_2O_2} = \frac{E_p\varepsilon_{H_2O_2}[1-10^{-(a+\varepsilon_{H_2O_2}[H_2O_2])z}]}{(a+\varepsilon_{H_2O_2}[H_2O_2])z} \quad (4)$$

where E_p (Es cm^{-2} s^{-1}) is the incident photon irradiance at the water surface, $\varepsilon_{H_2O_2}$ (M^{-1}cm^{-1}) is the molar absorption coefficient of H$_2$O$_2$, a (cm^{-1}) is the measured sample absorbance, and z (cm) is the sample depth. The direct photolysis rate constant, k'_d, can be calculated using equation 6.

$$\frac{-d[C]}{dt} = k'_d[C] = k_s \Phi[C] \qquad (1)$$

here, k_s (Es mol^{-1}sec^{-1}) is the specific rate of light absorbed by the chemical and Φ_C (mol Es^{-1}) is the chemical quantum yield. k_s can then be determined by equation 7:

$$k_s = \frac{E_p \varepsilon_c [1 - 10^{-az}]}{az} \qquad (2)$$

where ε_C (M^{-1}cm^{-1}) is the chemical molar absorption coefficient and the rest of the terms have been defined.

Figure 6 compares the experimental, k'obs, and predicted, k'model, rate constants for LCT and well water.
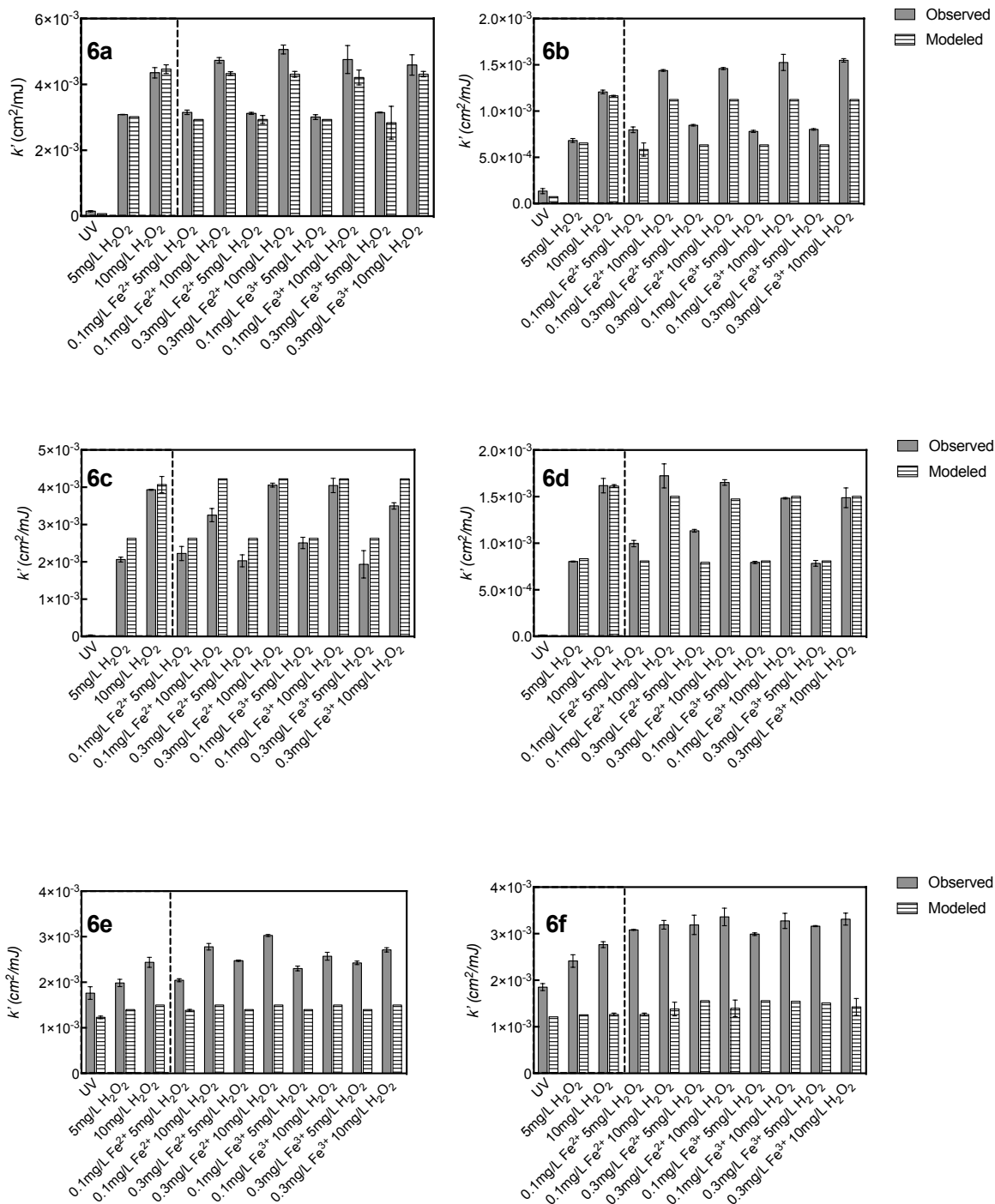
Figure 6. A comparison between observed and modeled pseudo-first order reaction rate constants for pCBA (6a, 6b), CBZ (6c, 6d) and NDMA (6e, 6f) in LCT water (left) and well water (right). The y-axis is fit to scale. Error bars represent the standard deviations between duplicate experiments.

Control scenarios, UV, UV + 5 mg/L H_2O_2 and UV + 10 mg/L H_2O_2, for pCBA and CBZ observed and modeled reaction rates are in good agreement for well water, however, the model slightly over predicts observed CBZ degradation by approximately 5-10% in LCT water. There is considerable discrepancy between modeled and observed NDMA reaction rate constants (Figure 6e/6f). LCT and well water modeled results for control experiments were off by approximate factors of 1.4 and 1.6, respectively, when compared to experimental results for UV/H_2O_2 without iron. Since NDMA is the only selected chemical that degrades primarily through direct photolysis, there is a strong likelihood of an error in the model calculations related to direct photolysis, k'_d. Additional explanation is provided in Appendix K.

For the reasons provided in previous sections, deviations between experimental and modeled reaction rates with iron addition are more predominant in well water as shown for pCBA and CBZ, Figure 6a/6b and 6c/56d, respectively. pCBA experimental scenarios with iron are consistently 20% higher than $k'model$ in well water. Modeled results demonstrate that photo-Fenton reactions are chemical specific. Therefore, a uniform factor cannot be used to account for enhanced chemical removal in iron-enhanced UV/H_2O_2 systems.

The Influence of Iron on NDMA Removal

NDMA was the only chemical where iron addition improved removal rates in LCT and well water. Furthermore, NDMA degradation rate constants were consistently higher in well water despite higher ˙OH scavenging potential. Two hypotheses can be proposed to explain these results. First, a unique oxidant produced during photo-Fenton reacts more strongly with NDMA than cyclic or aromatic chemicals with high second order hydroxyl radical rate constants. Using NDMA as a probe compound, Wink et al. published evidence of an oxidative species produced concurrently with ˙OH in dark and acidic Fenton reactions. Results from stop-flow spectrophotometry (Wink et al., 1991) and quenching studies (Wink et al., 1994) suggest 'transient A' is the predominant radical responsible for NDMA removal. Bossmann et al. also provided evidence that ˙OH contribution was minimal when compared to the oxidative specie ferryl in Fenton reaction (Bossmann et al., 1988). Byproducts of dimethylanilines after thermal and photo-assisted Fenton reactions were compared to UV/H_2O_2. Hydroxylated anilines were formed only after UV/H_2O_2, but not after Fenton treatment. Literature published later (Pignatello et al., 1999, Vermilyea and Voelker, 2009) again gave evidence to a transient specie, ferryl, produced in classical Fenton and neutral pH photo-Fenton reactions. Ferryl's contribution

was minimal when compared to ˙OH. However, since Wink et al., NDMA has not been used as a probe compound in Fenton experiments. Whether 'transient A' and ferryl are the same oxidant is yet to be determined.

To test this hypothesis, a kinetics experiments using tert-butyl alcohol (t-BuOH) as an HO˙ competitor, which has a low reaction rate with ferryl (Pignatello et al., 2006), and NDMA as the probe could be conducted. An experimental plan is provided in Appendix L.

Second, NDMA could be complexing with iron or, in the case of well water, other cations present in the water matrix. Separate time-based experiments were performed to better understand NDMA removal in the presence of iron and UV without H_2O_2 addition. Results are illustrated in Figure 7. Similar to trends observed for fluence-based degradation rate constants, NDMA removal rates were once again higher in well water than LCT water.
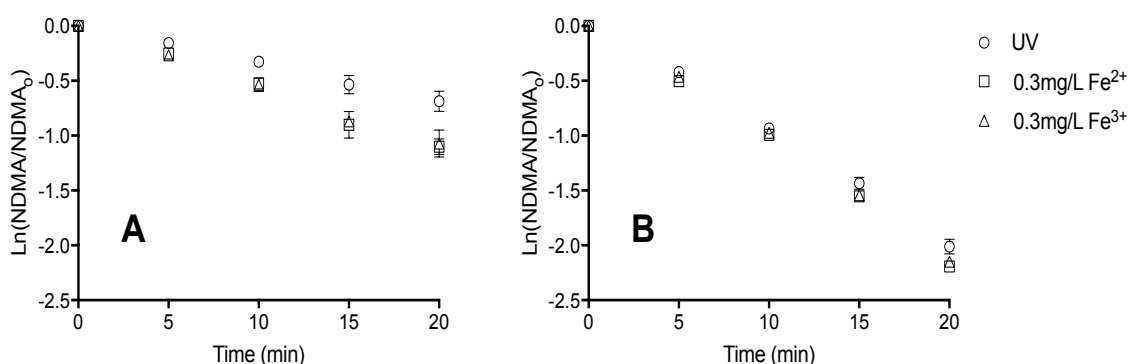
Figure 7. Degradation of NDMA in LCT (A) and well (B) water over time.

Compared to UV photolysis alone, iron addition increased NDMA removal by 38% in LCT water and 8% in well water. Results demonstrate dependency on the water matrix which indicates NDMA may act as a sequestering agent for cation complexation. Lone electrons on the nitrogens may provide viable coordination sites for iron. NDMA could undergo an electron distribution shift after complexation resulting in a more susceptible compound to photolysis and HO˙ oxidation. In addition to iron, magnesium and calcium, common cations found in ground water and present in the well water at 74 mg/L Ca^{2+} and 30 mg/L Mg^{2+}, maybe also be complexing with NDMA. This, along with more stable iron carbonate complexes formed in well water, would explain why UV photolysis reaction rates in well water are 65% higher than in LCT water. Interestingly, equal NDMA removal was achieved with Fe(II) and Fe(III) for LCT

and well water. This suggests Fe(II) was immediately oxidized by HO˙ to Fe(III). To test if cations are affecting NDMA direct and indirect photolysis rates, an additional experiment could be conducted where magnesium, calcium and iron are added individually and incrementally to low-carbon water, such as LCT, containing NDMA and exposed to UV light.

Conclusion

This study demonstrates that low levels of iron can enhance chemical removal in UV/H_2O_2 systems at neutral pH. Iron-assisted UV/H_2O_2 efficiency was most influenced by photochemical and kinetic properties of the target chemical and the water matrix. For iron-assisted UV/H_2O_2 tests conducted in well water, a 20% increase in HO˙ production was observed using the radical probe compound pCBA, and degradation rates increased for all pCBA and NDMA test scenarios up to 22% and 24%, respectively.

NDMA was the only chemical where iron addition improved removal rates in LCT and well water. Furthermore, iron without H_2O_2 addition was shown to increase NDMA removal by 38% in LCT water and 8% in well water when compared to UV photolysis alone. These results suggest NDMA could be forming a complex with iron, or in the case of well water other existing cations, and creating a more photoliable compound.

Diverse chemical reactions to iron-assisted UV/H_2O_2 in LCT and well water indicate photo-Fenton reactions are chemical-specific and rely on the water matrix. Chemical removal efficiencies with iron addition were not uniform, as demonstrated when modeled and experimental results were compared for pCBA and CBZ. Contradictory to previous literature, iron concentration, iron species and hydrogen peroxide concentration did not appear to impact chemical removal. Given the low levels of iron used in this study, the fraction of iron able to participate in photo-Fenton reactions, or potentially form a complex with the target compound, was most likely determined by the formation of stable iron complexes.

References

Aldrich, A.P., van den Berg, C.M., Thies, H., Nickus, U., 2001. The redox speciation of iron in two lakes. Mar. Freshw. Res. 52, 885–890.

Bauer, R., Fallmann, H., 1997. The photo-Fenton oxidation-a cheap and efficient wastewater treatment method. Res. Chem. Intermed. 23, 341–354.

Bautz, J., Bukowski, M.R., Kerscher, M., Stubna, A., Comba, P., Lienke, A., Münck, E., Que, L., 2006. Formation of an Aqueous Oxoiron(IV) Complex at pH 2–6 from a Nonheme Iron(II) Complex and H2O2. Angew. Chem. Int. Ed. 45, 5681–5684. doi:10.1002/anie.200601134

Bernabeu, A., Palacios, S., Vicente, R., Vercher, R.F., Malato, S., Arques, A., Amat, A.M., 2012. Solar photo-Fenton at mild conditions to treat a mixture of six emerging pollutants. Chem. Eng. J. 198–199, 65–72. doi:10.1016/j.cej.2012.05.056

Buxton, G.V., Greenstock, C.L., Helman, W.P., Ross, A.B., Tsang, W., 1988. Critical Review of rate constants for reactions of hydrated electronsChemical Kinetic Data Base for Combustion Chemistry. Part 3: Propane. J. Phys. Chem. Ref. Data 17, 513. doi:10.1063/1.555805

Chen, R., Pignatello, J.J., 1997. Role of quinone intermediates as electron shuttles in Fenton and photoassisted Fenton oxidations of aromatic compounds. Environ. Sci. Technol. 31, 2399–2406.

Chong, M.N., Jin, B., Chow, C.W.K., Saint, C., 2010. Recent developments in photocatalytic water treatment technology: A review. Water Res. 44, 2997–3027. doi:10.1016/j.watres.2010.02.039

De la Cruz, N., Esquius, L., Grandjean, D., Magnet, A., Tungler, A., de Alencastro, L.F., Pulgarín, C., 2013. Degradation of emergent contaminants by UV, UV/H2O2 and neutral photo-Fenton at pilot scale in a domestic wastewater treatment plant. Water Res. 47, 5836–5845. doi:10.1016/j.watres.2013.07.005

De la Cruz, N., Giménez, J., Esplugas, S., Grandjean, D., de Alencastro, L.F., Pulgarín, C., 2012. Degradation of 32 emergent contaminants by UV and neutral photo-fenton in domestic wastewater effluent previously treated by activated sludge. Water Res. 46, 1947–1957. doi:10.1016/j.watres.2012.01.014

Doumic, L.I., Soares, P.A., Ayude, M.A., Cassanello, M., Boaventura, R.A.R., Vilar, V.J.P., 2015. Enhancement of a solar photo-Fenton reaction by using ferrioxalate complexes for the treatment of a synthetic cotton-textile dyeing wastewater. Chem. Eng. J. 277, 86–96. doi:10.1016/j.cej.2015.04.074

Gallard, H., De Laat, J., 2000. Kinetic modelling of Fe(III)/H2O2 oxidation reactions in dilute aqueous solution using atrazine as a model organic compound. Water Res. 34, 3107–3116. doi:10.1016/S0043-1354(00)00074-9

Katsoyiannis, I.A., Canonica, S., von Gunten, U., 2011. Efficiency and energy requirements for the transformation of organic micropollutants by ozone, O3/H2O2 and UV/H2O2. Water Res. 45, 3811–3822. doi:10.1016/j.watres.2011.04.038

Keenan, C.R., Sedlak, D.L., 2008. Factors Affecting the Yield of Oxidants from the Reaction of Nanoparticulate Zero-Valent Iron and Oxygen. Environ. Sci. Technol. 42, 1262–1267. doi:10.1021/es7025664

Keen, O.S., Baik, S., Linden, K.G., Aga, D.S., Love, N.G., 2012. Enhanced Biodegradation of Carbamazepine after UV/H$_2$O$_2$ Advanced Oxidation. Environ. Sci. Technol. 46, 6222–6227. doi:10.1021/es300897u

King, D.W., Farlow, R., 2000. Role of carbonate speciation on the oxidation of Fe(II) by H2O2. Mar. Chem. 70, 201–209. doi:10.1016/S0304-4203(00)00026-8

Klamerth, N., Rizzo, L., Malato, S., Maldonado, M.I., Agüera, A., Fernández-Alba, A.R., 2010. Degradation of fifteen emerging contaminants at µg L−1 initial concentrations by mild solar photo-Fenton in MWTP effluents. Water Res., Emerging Contaminants in water: Occurrence, fate, removal and assessment in the water cycle (from wastewater to drinking water) 44, 545–554. doi:10.1016/j.watres.2009.09.059

Klassen, Normal V., David Marchington, and Heather C.E. McGowan. "H2O2 Determination by the I3- Method and by KMnO4 Titration." *Analytical Chemistry* 66, no. 18 (September 1, 1994): 2921–25. doi:10.1021/ac00090a020.

Lutterbeck, C.A., Wilde, M.L., Baginska, E., Leder, C., Machado, Ê.L., Kümmerer, K., 2015. Degradation of 5-FU by means of advanced (photo)oxidation processes: UV/H2O2, UV/Fe2 +/H2O2 and UV/TiO2 — Comparison of transformation products, ready biodegradability and toxicity. Sci. Total Environ. 527–528, 232–245. doi:10.1016/j.scitotenv.2015.04.111

Mártire, D.O., Caregnato, P., Furlong, J., Allegretti, P., Gonzalez, M.C., 2002. Kinetic study of the reactions of oxoiron(IV) with aromatic substrates in aqueous solutions: Kinetic Study of the Reactions of Oxoiron(IV). Int. J. Chem. Kinet. 34, 488–494. doi:10.1002/kin.10076

Minero, C., Lucchiari, M., Maurino, V., Vione, D., 2013. A quantitative assessment of the production of ˙OH and additional oxidants in the dark Fenton reaction: Fenton degradation of aromatic amines. RSC Adv. 3, 26443. doi:10.1039/c3ra44585b

Neamţu, M., Grandjean, D., Sienkiewicz, A., Le Faucheur, S., Slaveykova, V., Colmenares, J.J.V., Pulgarín, C., de Alencastro, L.F., 2014. Degradation of eight relevant micropollutants in different water matrices by neutral photo-Fenton process under UV254 and simulated solar light irradiation − A comparative study. Appl. Catal. B Environ. 158–159, 30–37. doi:10.1016/j.apcatb.2014.04.001

Nieto-Juarez, J.I., Pierzchła, K., Sienkiewicz, A., Kohn, T., 2010. Inactivation of MS2 coliphage in Fenton and Fenton-like systems: role of transition metals, hydrogen peroxide and sunlight. Environ. Sci. Technol. 44, 3351–3356. doi:10.1021/es903739f

Oppenlander (2003) Photochemical Purification of Water and Air, Wiley VCH, Weinheim Germany

Ortega-Gómez, E., Martín, M.M.B., García, B.E., Pérez, J.A.S., Ibáñez, P.F., 2016. Wastewater disinfection by neutral pH photo-Fenton: The role of solar radiation intensity. Appl. Catal. B Environ. 181, 1–6. doi:10.1016/j.apcatb.2015.06.059

Pérez, M., Torrades, F., Domènech, X., Peral, J., 2002. Fenton and photo-Fenton oxidation of textile effluents. Water Res. 36, 2703–2710. doi:10.1016/S0043-1354(01)00506-1

Pignatello, J.J., Liu, D., Huston, P., 1999. Evidence for an Additional Oxidant in the Photoassisted Fenton Reaction. Environ. Sci. Technol. 33, 1832–1839. doi:10.1021/es980969b

Pignatello, J.J., Oliveros, E., MacKay, A., 2006. Advanced Oxidation Processes for Organic Contaminant Destruction Based on the Fenton Reaction and Related Chemistry. Crit. Rev. Environ. Sci. Technol. 36, 1–84. doi:10.1080/10643380500326564

Rahim Pouran, S., Abdul Aziz, A.R., Wan Daud, W.M.A., 2015. Review on the main advances in photo-Fenton oxidation system for recalcitrant wastewaters. J. Ind. Eng. Chem. 21, 53–69. doi:10.1016/j.jiec.2014.05.005

Rosenfeldt, E.J., Linden, K.G., 2007. The $R_{OH,UV}$ Concept to Characterize and the Model UV/H_2O_2 Process in Natural Waters. Environ. Sci. Technol. 41, 2548–2553. doi:10.1021/es062353p

Rubio, D., Nebot, E., Casanueva, J.F., Pulgarin, C., 2013. Comparative effect of simulated solar light, UV, UV/H2O2 and photo-Fenton treatment (UV–Vis/H2O2/Fe2+,3+) in the Escherichia coli inactivation in artificial seawater. Water Res. 47, 6367–6379. doi:10.1016/j.watres.2013.08.006

Sharpless, C.M., Linden, K.G., 2003. Experimental and Model Comparisons of Low- and Medium-Pressure Hg Lamps for the Direct and H_2O_2 Assisted UV Photodegradation of N-Nitrosodimethylamine in Simulated Drinking Water. Environ. Sci. Technol. 37, 1933–1940. doi:10.1021/es025814p

Southworth, B.A., Voelker, B.M., 2003. Hydroxyl Radical Production via the Photo-Fenton Reaction in the Presence of Fulvic Acid. Environ. Sci. Technol. 37, 1130–1136. doi:10.1021/es020757l

Sun, L., Qian, J., Blough, N.V., Mopper, K., 2015. Insights into the Photoproduction Sites of Hydroxyl Radicals by Dissolved Organic Matter in Natural Waters. Environ. Sci. Technol. Lett. doi:10.1021/acs.estlett.5b00294

Sun, Y., Pignatello, J.J., 1992. Chemical treatment of pesticide wastes. Evaluation of iron (III) chelates for catalytic hydrogen peroxide oxidation of 2, 4-D at circumneutral pH. J. Agric. Food Chem. 40, 322–327.

Swaim, P., Royce, A., Smith, T., Maloney, T., Ehlen, D., Carter, B., 2008. Effectiveness of UV Advanced Oxidation for Destruction of Micro-Pollutants. Ozone Sci. Eng. 30, 34–42. doi:10.1080/01919510701753390

Teel, A.L., Warberg, C.R., Atkinson, D.A., Watts, R.J., 2001. Comparison of mineral and soluble iron Fenton's catalysts for the treatment of trichloroethylene. Water Res. 35, 977–984. doi:10.1016/S0043-1354(00)00332-8

Velo-Gala, I., López-Peñalver, J.J., Sánchez-Polo, M., Rivera-Utrilla, J., 2014. Comparative study of oxidative degradation of sodium diatrizoate in aqueous solution by H2O2/Fe2+, H2O2/Fe3+, Fe (VI) and UV, H2O2/UV, K2S2O8/UV. Chem. Eng. J. 241, 504–512. doi:10.1016/j.cej.2013.10.036

Vermilyea, A.W., Voelker, B.M., 2009. Photo-Fenton Reaction at Near Neutral pH. Environ. Sci. Technol. 43, 6927–6933. doi:10.1021/es900721x

Vione, D., Minella, M., Maurino, V., Minero, C., 2014a. Indirect Photochemistry in Sunlit Surface Waters: Photoinduced Production of Reactive Transient Species. Chem. - Eur. J. 20, 10590–10606. doi:10.1002/chem.201400413

Vione, D., Minella, M., Maurino, V., Minero, C., 2014b. Indirect Photochemistry in Sunlit Surface Waters: Photoinduced Production of Reactive Transient Species. Chem. - Eur. J. 20, 10590–10606. doi:10.1002/chem.201400413

Wink, D.A., Nims, R.W., Desrosiers, M.F., Ford, P.C., Keefer, L.K., 1991. A kinetic investigation of intermediates formed during the Fenton reagent mediated degradation of N-nitrosodimethylamine: evidence for an oxidative pathway not involving hydroxyl radical. Chem. Res. Toxicol. 4, 510–512.

Wink, D.A., Nims, R.W., Saavedra, J.E., Utermahlen, W.E., Ford, P.C., 1994a. The Fenton oxidation mechanism: reactivities of biologically relevant substrates with two oxidizing intermediates differ from those predicted for the hydroxyl radical. Proc. Natl. Acad. Sci. 91, 6604–6608.

Wink, D.A., Wink, C.B., Nims, R.W., Ford, P.C., 1994b. Oxidizing intermediates generated in the Fenton reagent: kinetic arguments against the intermediacy of the hydroxyl radical. Environ. Health Perspect. 102, 11.

Wols, B.A., Hofman-Caris, C.H.M., 2012. Review of photochemical reaction constants of organic micropollutants required for UV advanced oxidation processes in water. Water Res. 46, 2815–2827. doi:10.1016/j.watres.2012.03.036

Zepp, R.G., Faust, B.C., Hoigne, J., 1992. Hydroxyl radical formation in aqueous reactions (pH 3-8) of iron (II) with hydrogen peroxide: the photo-Fenton reaction. Environ. Sci. Technol. 26, 313–319.

Appendix A: Fenton and photo-Fenton Literature Review

Overview of Fenton and photo-Fenton Reactions

In 1894 Henry Fenton's research efforts lead to the discovery of the classical Fenton reagent, a mixture of hydrogen peroxide (H_2O_2) and Ferrous (Fe(II)) iron under acidic conditions (pH <3). Fenton witnessed the oxidation of Tararic acid, which was by hydroxyl radical ($\cdot$OH) interactions, a later identified transient byproduct. The active oxidant, $\cdot$OH, can be achieved under dark (dark Fenton) or light (photo-Fenton) environments. Widely accepted $\cdot$OH generation in dark-Fenton systems in the absence of ligands follows the mechanism chain presented in eqs 1-4:

$$Fe^{2+} + H_2O_2 \rightarrow Fe^{3+} + HO^- + HO^\cdot \quad (1)$$
$$Fe^{3+} + H_2O_2 \rightarrow Fe^{2+} + HO_2^\cdot + H^+ \quad (2)$$
$$HO^\cdot + H_2O_2 \rightarrow HO_2^\cdot + H_2O \quad (3)$$
$$HO^\cdot + Fe^{2+} \rightarrow Fe^{3+} + HO^- \quad (4)$$
$$Fe^{3+} + HO_2^\cdot \rightarrow Fe^{2+} + O_2 + H^+ \quad (5)$$
$$Fe^{2+} + HO_2^\cdot + H^+ \rightarrow H_2O_2 + Fe^{3+} \quad (6)$$
$$HO_2^\cdot + HO_2^\cdot \rightarrow H_2O_2 + O_2 \quad (7)$$
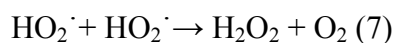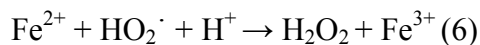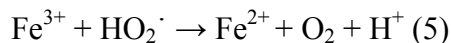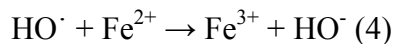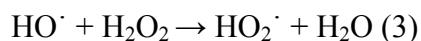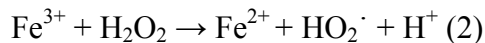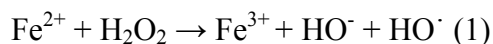
Soluble ferrous and ferric iron are cycled autocatalytically to produce (1) and consume (3, 4) $\cdot$OH radicals.

Photoassisted Fenton (photo-Fenton) reactions take place under ultraviolet (UV) or UV/visible light, eqs 8-9. Sample irradiation has been shown to enhance $\cdot$OH formation directly from H_2O_2 photolysis (8), Fe(III) photo-reactions (9) and indirectly from regenerating Fe(II) (10). Ferric iron is solely responsible for reactions 9-10. When exposed to a light source, ferric iron can undergo photoreduction to ferrous iron form complexes via ligand-to-metal charge transfer excitation (9). Ferrous iron then participates in reaction 1 and hydroxyl radicals are generated.

$$H_2O_2 + h\nu \rightarrow 2HO^\cdot \quad (8)$$
$$Fe^{3+}(L)_n + h\nu \rightarrow Fe^{2+}(L)_{n-1} + L^\cdot \quad (9)$$
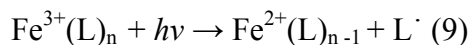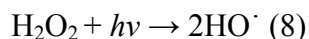
For mechanism 9, Fe(III) can form stable organo complexes with natural organic matter (NOM) present in surface and ground waters. This is especially important for systems at neutral pH because these complexes typically have higher molar absorption coefficients and quantum yields in the near UV and visible regions (Pignatello et al., 2006). Measured quantum yields are shown in Table 5 (Oppenlander, 2002).

Table 5. Measured iron quantum yields for different wavelengths.

Primary Iron Specie Measured	Irradiation wavelength (nm)	Quantum yield
Fe^{2+}	220-600	1.32
Fe^{2+}	220-600	0.21
Fe^{2+}+ OH	313	0.14

Parameters Known to Influence Fenton Reactions

The Fenton process can achieve micropollutant oxidation spontaneously in natural systems (Vermilyea and Voelker, 2009) or engineered for industrial processes (De la Cruz et al., 2013). Within these applications, classical Fenton reagent parameters and optimized parameters have been extensively explored and mainly include pH, H_2O_2 concentration, iron to H_2O_2 ratio, iron species, and retention time. Photo-Fenton researchers have included varied light sources, intensities and wavelengths. The broad consensus is optimal pH conditions are around 3, and generally higher H_2O_2 to iron ratios, light intensities and contact times produce efficient Fenton processes (Pignatello et al., 2006).

Effect of pH

Fenton and photo-Fenton processes have been most commonly explored under acidic conditions (pH <3) utilizing Fe(III) and Fe(II) hexaquo complexes, $[FeOH(H_2O))^6]^{3+}$ and $[FeOH(H_2O))^5]^{2+}$, respectively (Pignatello et al., 2006,Vermilyea and Voelker, 2009). Exceeding a pH of 3 results in a less Fenton-reactive system due to Fe(III) precipitation via hydrolysis (Sun and Pignatello, 1992). While Fe(II) salts are soluble in water even at neutral pH, ferrous iron will co-precipitate in the presence of ferric hydroxides and oxygen. Despite the formation of colloidal iron, Fe(III) and Fe(II) hydroxides under neutral pH conditions can still partake in the Fenton reaction (Southworth and Voelker, 2003, King and Farlow, 2000, Aldrich et al., 2001). To maintain Fenton reactivity under neutral pH conditions, researchers have used heterogeneous or homogeneous catalysts to stabilize Fe^{3+} thereby preventing Fe(III) hydroxide precipitation

(Rahim Pouran et al., 2015, Sun and Pignatello, 1992). Utilization of catalysts have several draw backs including having to remove or re-generate the catalysis, enhanced toxicity, and overall increased costs (Rahim Pouran et al., 2015).

Several studies (Klamerth et al., 2010, Ortega-Gómez et al., 2016,Vermilyea and Voelker, 2009, Bernabeu et al., 2012, Southworth and Voelker, 2003, Rubio et al., 2013, De la Cruz et al., 2012, 2013,Vione et al., 2014, Neamţu et al., 2014, Velo-Gala et al., 2014) have used photo-Fenton to degrade micropollutants without catalyst assistance at circumneutral pH. Bernabeu et al. determined neutral solar photo-Fenton conditions were two orders of magnitude less efficient than acidic photo-Fenton reactions, however, iron addition overall enhanced chemical degradation. Klamerth et al. successfully degraded 15 organic compounds using solar Fenton at neutral pH using 5 mg/L Fe and varied H_2O_2 (50 mg/L - 5 mg/L) and found Fenton efficiencies were dependent on ˙OH radical scavengers present in the water matrix and independent of H_2O_2 concentration. Both research studies commented on the impact the aqueous water matrix has on the Fenton process. Humic acids, inorganic salts, and carbonates were observed to inhibit solar photo-Fenton radical production.

Effect of Hydrogen Peroxide Concentration

While Klamerth et al. found enhanced hydrogen peroxide concentration did not increase chemical removal, Nieto-Juarez et. al demonstrated linear dependence on H_2O_2 concentration between 0 and 50 uM for solar Fenton virus inactivation (Nieto-Juarez et al., 2010). Under acidic dark Fenton conditions, Gallard and De Laat determined the impact of H_2O_2 concentration can be divided into three regions as shown in Figure 11 (Pignatello et al., 2006). From 0 to 10 mM H_2O_2 ATZ follows first order kinetics, 10 mM to 50 mM H_2O_2 the reaction becomes zeroth order due to ˙OH scavenging by H_2O_2, and finally concentrations greater than 50 mM H_2O_2 inhibit chemical degradation from ˙OH scavenging and Fe(III)–peroxo complex formation (a less active iron species) (Pignatello et al., 2006).
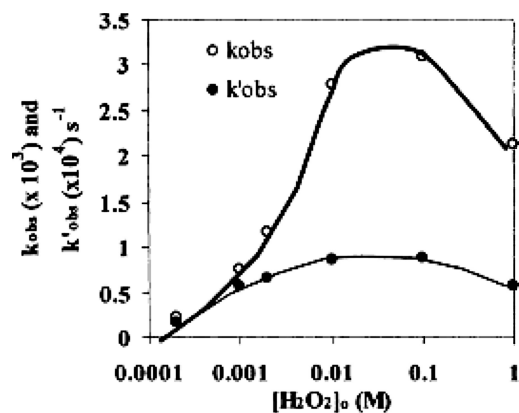
Figure 8. Influence of initial [H2O2] on the observed rate constant for reaction of atrazine in the Fenton reaction at pH 3. From Gallard and De Latt, 2000.

Iron Stability

Iron can form strong ligands with Ethylenediaminetetraacetic acid (EDTA), phosphate ion (PO_4^3), cyanide (CN), carbonate species (CO_3^{2-}) and weak ligands with Fluorine (F^-), Chlorine (Cl^-) and sulfate (SO_4^{2-}). In the absence of named ions, iron will a form metal-ligand complexes with hydroxide ions. Hydro-complex formation is pH dependent and unique to the metal species. In addition to pH, carbonates in solution with hydrogen peroxide can change iron speciation for a pH> 5 $Fe(CO)_3$ (King and Farlow, 2000). Fe(II) and Fe(III) hydroxo-complex formations and corresponding equilibrium constants are represented in Appendix B. The primary iron species present at neutral pH are Fe(III) hydroxides $[Fe(OH)]_2^+$, also referred to as peroxo complexes. The rate at which peroxo complexes are formed is enhanced by H_2O_2 addition (Velo-Gala et al., 2014). The propensity of some chelating ligands (polycarboxylates, citrate, oxalic or gluconic acid) forming complexes with iron at neutral pH will depend on the water matrix. Within a neutral pH range (6.5 to 7.8) typical of natural systems, and used in this study, all iron species were in colloidal form. This was also the case for De la Cruz et al. were iron remained undissolved throughout UV_{254nm} photo-Fenton processes.

In aqueous solutions without the presence of hydrogen peroxide iron has been shown to react with, and in some cases oxidize, organic compounds, mainly organoperoxides, hydroquinones, and certain dyes (Pignatello et al., 2006). It should be noted that neither Fe(II) ion or Fe(III) aquo-ligands are very reactive. Fe(II) is a weak reductant while Fe(III) aquo complexes are poor oxidants.

Studies, similar to the one herein, evaluated the photo-Fenton at neutral pH employing UV$_{254nm}$ for chemical oxidation (De la Cruz et al., 2012, De la Cruz et al., 2013, Neamţu et al., 2014; Velo-Gala et al., 2014). With the exception of De la Cruz et al. (2012), all studies were comparative assessments of Fenton and photo-Fenton processes at neutral pH. A brief summary of UV$_{254nm}$ Photo-Fenton parameters explored within these studies is provided in Table 6.

Table 6. Experimental parameters for UV$_{254}$ photo-Fenton studies conducted at neutral pH.

Reference	H$_2$O$_2$ (mg/L)	Iron (mg/L)	Initial Iron Specie	TOC (mg/L)	pH
N. De la Cruz et al., 2013	20-50	0-4	Ferrous	5 - 7.5	6-7
Neamtu, et al., 2014	~10-20	1.7-3.3	Ferrous	1540	6.5
N. De la Cruz et al., 2012	10-50	0-5	Ferrous/Ferric	15.93	7.42
Velo-Gala et al., 2014	5-50	0.1-50	Ferric	~5-21	6.5

Whether or not a photochemical reaction would take place in a Fenton system depends on the light-source intensity and emission spectra, absorbance, concentration and quantum yield of the target chemical, and other absorbable species present in the system (Pignatello et al., 2006).

The Influence of Iron and Hydrogen Peroxide Concentration

A pilot study conducted by De la Cruz et al. showed that increased iron concentration did not significantly increase pollutant removal. Furthermore, at lower hydrogen peroxide concentrations iron addition inhibited chemical reduction. The following example was provided: at 30 mg/L H$_2$O$_2$, average chemical degradation rates for 0, 2 and 4 mg/L of added Fe^{3+}, respectively, were 83, 83 and 84%; at 30 mg/L H$_2$O$_2$, average degradation rates 0, 2 and 4 mg/L of added Fe^{3+} were 74, 62 and 61%. These results were explained by attributing decreased the UV transmittance with increased iron which in turn decreased the UV intensity within the reactor. At higher iron concentrations, UV light was shielded from hydrogen peroxide and target chemicals, some of which degraded through direct photolysis. This is commonly referred to as "inter-filter effects," where light absorbable iron and other light absorbable organic species block photolysis of the target contaminant or hydrogen peroxide. An alternative explanation, not

discussed, is that the molar ratios of H_2O_2 to iron catalyst fell below or above reported optimal ratios of 10:1 to 40:1 (Pérez et al., 2002).

Radical Species Present in Fenton Reactions

Radical species identified during Fenton processes are the hydroxyl radical ($\cdot$OH), peroxyl radical (ROO$\cdot$), the hydroperoxyl radical (HO$_2\cdot$) and its conjugated base, the superoxide anion ($O_2^{\cdot-}$). The radicals mentioned above are inherent to all advanced oxidation processes (AOPs). AOPs rely mainly on the non-selective, highly reactive $\cdot$OH oxidant ($E_o = 2.80$ V) for most organic chemical destruction (Katsoyiannis et al., 2011). Second order rate constants of organic chemicals range from 10^7 to 10^{10} $M^{-1}s^{-1}$ (Wols and Hofman-Caris, 2012, Buxton et al., 1988). The non-selective behavior of $\cdot$OH results in oxidation of constituents other than the target compound, hence why water matrices with low scavenging potential (i.e. low carbonates, nitrite, and organics) are ideal. Three main mechanisms of chemical (C) oxidation via $\cdot$OH have are acknowledged (Oppenlander, 2002): electron transfer (11), hydrogen abstraction (12) and electrophilic addition (13).

$\cdot$OH + C^n $\rightarrow$ C^{n+1} + HO$^-$ (11)
$\cdot$OH + R-H $\rightarrow$ R$\cdot$ + H_2O (12)
$\cdot$OH + $R_2C=\cdot CR_2$—C(OH)R$_2$ (13)
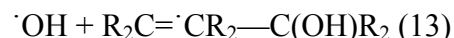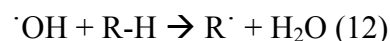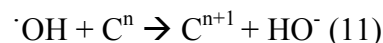
Literature often uses $\cdot$OH production as a primary parameter for Fenton efficiency (Zepp et al., 1992, Gallard and De Laat, 2000, Southworth and Voelker, 2003, Lutterbeck et al., 2015, De la Cruz et al., 2012).

Reactive species unique to the Fenton process particularly at neutral pH are iron-oxo species, mainly the ferryl ion, FeO_2^+ (Keenan and Sedlak, 2008, Minero et al., 2013, Bauer and Fallmann, 1997, Mártire et al., 2002, Vione et al., 2014b). $\cdot$OH and ferryl are said to be produced concurrently in Fenton reactions and utilize similar mechanisms for chemical degradation, pathways 11-13, which can vary in the literature (Pignatello et al., 1999, Mártire et al., 2002). Ferryl is hypothesized to form when Fe(II) or Fe(III) are chelated with specific ligands (pathway 10); chelating agents identified by Pignatello are polycarboxylate or macrocyclic ligands. The literature is in good agreement on $\cdot$OH as the main oxidant present under acidic condition,

however, the ratio of ferryl to ˙OH at acidic and neutral conditions is debated. At a pH of 2, Minero et al. estimated 60% of 2,4- and 3,4-dichloroaniline and methyl yellow degradation was attributed to ˙OH and the remaining 40% attributed to another species hypothesized to be ferryl. The opposite is true for pH values typical of surface water where the OH yield for Fenton are shown to be much lower than 60% (Vermilyea and Voelker, 2009) indicating ferryl could be the main oxidizing species present.

The evidence for the existence of ferryl is strong and its contribution to chemical degradation cannot be refuted, the role of ferryl maybe trivial for photo-Fenton systems at neutral pH utilizing high light intensities and excess H_2O_2. Although his theory has yet to be tested, Ferryl second order reaction rate constants are 5 orders of magnitude lower than ˙OH with the exception of the nitrophenols, presented in Table 7.

Table 7. Second order ferryl and hydroxyl radical reaction rates of with select organic compounds.

Chemical	K_F ($M^{-1}s^{-1}$) x 10^4 (a)	K_{OH} ($M^{-1}s^{-1}$) x 10^9 (b)
Phenol	0.15 (± 0.2)	10.3 (±5.2)
m-nitrophenol	13.6 (± 0.9)	--
o-nitrophenol	5.8 (± 0.4)	--
Nitrobenzene	1.05 (± 0.2)	3.40 (±0.71)

(a) Mártire et al., 2002
(b) Wols and Hofman-Caris, 2012

Predicted Chemical Reactions for Selected Chemicals: pCBA, NDMA, CBZ

Despite evidence of ferryl production at neutral pH, the main reactive species responsible for chemical degradation in an UV_{254} photo-Fenton system is the hydroxyl radical when $H_2O_2 \gg Fe$. Whether or not iron addition enhances chemical degradation in UV/H_2O_2 systems seems to depend on the chemical of interest and light source. Out of the 32 organic chemicals analyzed by De la Cruz et al. (2012), only ciprofloxacin and terbutryn showed enhanced (20 and 40%, respectively) removal with 5 mg/L Fe^{2+} iron addition over UV/H_2O_2. Meanwhile, iron addition was shown to hinder ibuprofen, sotalol and mecoprop removal. Iron did not appear to enhance or inhibit Carbamazepine removal, which was the case for the remaining chemicals.

Para-Chlorobenzoic Acid

pCBA has two substituents para to each other. The polar carboxylic acid group is electron withdrawing (EWG) and directs potential substituents to the meta position. The para position contains a halogen, chloro group, an electron donating group (EDG) via resonance and EWG by polarity. Substituents are directed to the ortho/para position. The hydroxyl radical will undergo addition (pathway 13) with the aromatic ring by attacking carbon pi bonds, as proposed in Figure 9.
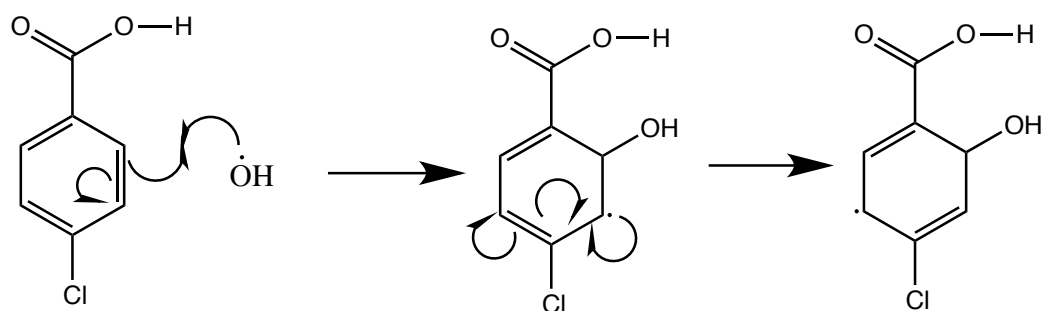
Figure 9. Proposed mechanism for hydroxyl radical attack on pCBA.

Carbamazepine

Two benzene rings on the outside with a centered seven membered ring containing a cyclic amine. Attached to the cyclic amine is an EWG polar amide. The pi electrons on the aromatic ring are good sites for hydroxyl radical addition (pathway 13), show in Figure 10 (Keen et al., 2012).
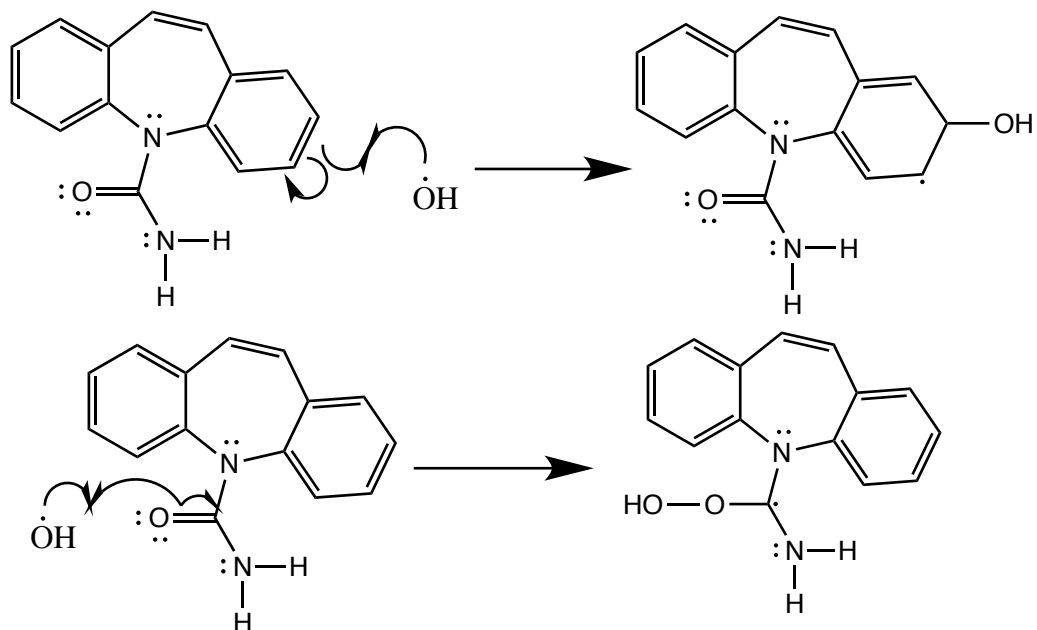
Figure 10. Proposed pathway for hydroxyl radical attack on CBZ.

N-Nitrosodimethylamine: HO˙ Oxidation

Two methyl groups are left with a partially positive charge due to the attached N-Nitroso group's polarity. NDMA oxidation by ˙OH is are not favored, however, one proposed ˙OH (Figure 11), is hydrogen abstraction from a methyl group (pathway 11). A second proposed ˙OH attack might be on the high-energy electrons on the nitroso group (pathway 11), shown in Figure 12.
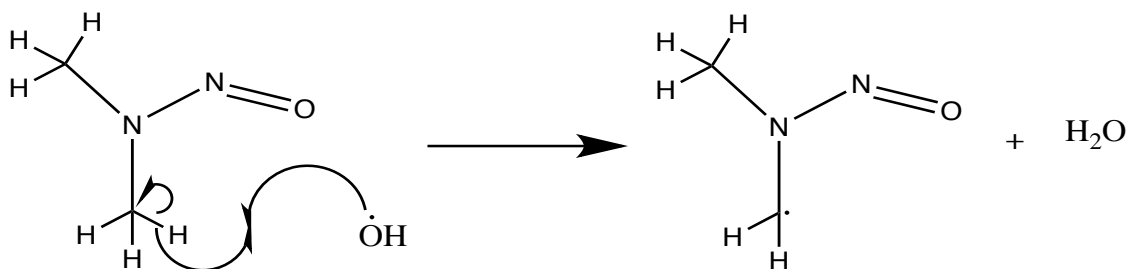
Figure 11. Proposed mechanism for hydroxyl radical attack on NDMA via hydrogen abstraction.
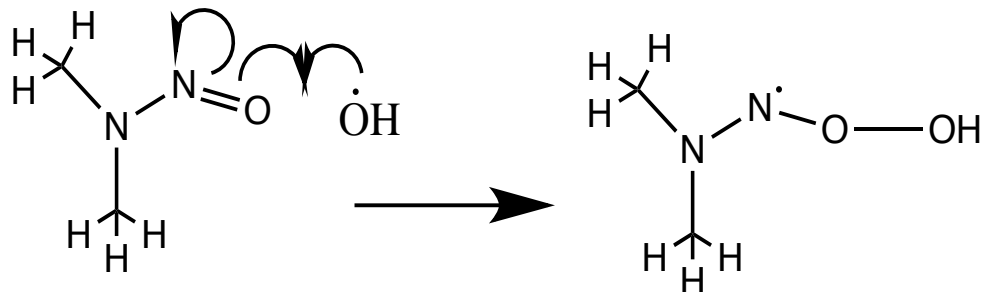
Figure 12. Proposed mechanism for hydroxyl radical attack on NDMA via electron addition.

N-Nitrosodimethylamine: Direct Photolysis

Well studied is the photolysis of NDMA. NDMA absorbs light between 200 and 275nm and has a relatively high quantum yield (0.30 mol/ einstein) at 254nm making low-pressure UV (LPUV) an effective treatment option (Sharpless and Linden, 2003). Owing to NDMA's chemical structure, degradation via ˙OH attack is not favored. Degradation through HO˙ attack is possible with a second order hydroxyl radical reaction rate constant of 3.8 x 10^8 $M^{-1}s^{-1}$ although when compared to pCBA and CBZ's reaction rate constants, it is an order of magnitude smaller.

N-Nitrosodimethylamine: Fenton Reactions

Limited literature is available on Fenton processes used to degrade NDMA. Using NDMA as a probe compound, Wink et al. published evidence of an oxidative species produced concurrently with ˙OH in dark and acidic Fenton reactions. A series of experiments using NDMA as a probe compound were conducted to prove, detect and differentiate radical species besides ˙OH produced in the Fenton process (Wink et al., 1991, 1994a, 1994b). Results from stop-flow spectrophotometry (Wink et al., 1991) and quenching studies (Wink et al., 1994) suggest 'transient A' is the main radical responsible for NDMA removal. Bossmann et al. also provided evidence that ˙OH contribution was minimal when compared to the oxidative specie, identified as Fe (IV) oxoiron, in Fenton reaction (Bossmann et al., 1988). Byproducts of dimethylanilines after thermal and photo-assisted Fenton reactions were compared to UV/H_2O_2. Hydroxylated anilines were formed only after UV/H_2O_2.

Literature published later (Pignatello et al., 1999, Vermilyea and Voelker, 2009) again gave evidence to a transient specie, ferryl, produced in dark, acidic Fenton and neutral pH photo-Fenton reactions although ˙OH was shown to be the main oxidant. In a competition kinetics

experiment using kinetic deuterium isotope effect (KDIE, defined as the rate change of a chemical reaction when a reactant's atom is replaced with one of its isotopes) using cyclohexane/cyclohexane-d$_{12}$, Pignatello et al. (1999) demonstrated with increasing t-BuOH (identified as a strong OH scavenger and weak ferry scavenger) at high t-BuOH levels no change in cyclohexane KDIE was witnessed in the UV/H$_2$O$_2$ system whereas cyclohexane KDIE activity was witnessed in the Fenton system. A figure take from Pignatello et al., 1999 representing this phenomenon is shown below in Figure 13.
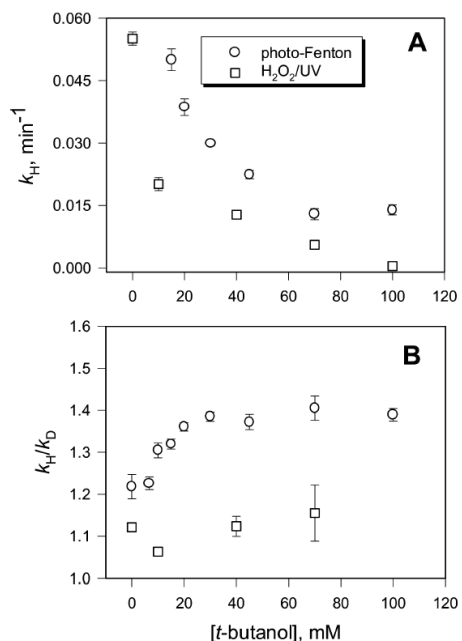
Figure 13. Reaction of cyclohexane KDIE under UV/H$_2$O$_2$ and photo-Fenton processes with increased t-BuOH. Figure take from Pignatello et al., 1999.

Appendix B: Visual Minteq Simulations

The following simulations were run using Visual MINTEQ software to illustrate iron speciation with respect to pH. Simulations were conducted using 0.3 mg/L Fe(II) and Fe(III) in LCT and well water. Redox Fe(II)/Fe(III) reactions were also run to simulate iron species present in LCT and well water. Ferric hydroxides were predominately present at neutral pH.
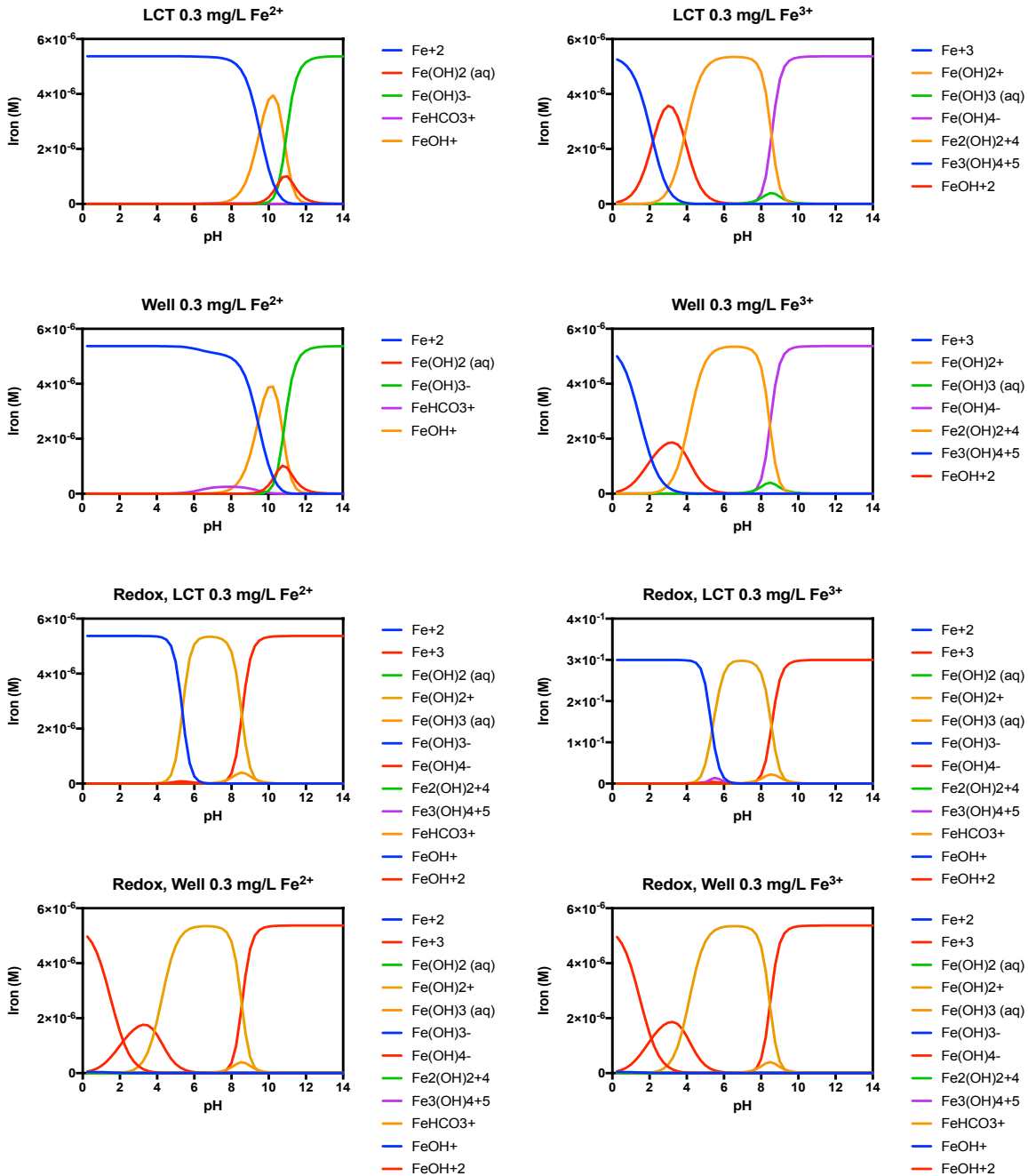
Appendix C: Test Matrix for UV/H_2O_2 and Iron-Assisted UV/H_2O_2 Experiments

The following test scenarios were carried in a collimated beam for UV-irradiated samples and in a light-impenetrable reactor for dark experiments.

Irradiated Experiments	Dark Experiments
UV	Dark
5mg/L H_2O_2	5mg/L H_2O_2
10mg/L H_2O_2	10mg/L H_2O_2
0.1mg/L Fe^{2+} 5mg/L H_2O_2	0.1mg/L Fe^{2+} 5mg/L H_2O_2
0.1mg/L Fe^{2+} 10mg/L H_2O_2	0.1mg/L Fe^{2+} 10mg/L H_2O_2
0.3mg/L Fe^{2+} 5mg/L H_2O_2	0.3mg/L Fe^{2+} 5mg/L H_2O_2
0.3mg/L Fe^{2+} 10mg/L H_2O_2	0.3mg/L Fe^{2+} 10mg/L H_2O_2
0.1mg/L Fe^{3+} 5mg/L H_2O_2	0.1mg/L Fe^{3+} 5mg/L H_2O_2
0.1mg/L Fe^{3+} 10mg/L H_2O_2	0.1mg/L Fe^{3+} 10mg/L H_2O_2
0.3mg/L Fe^{3+} 5mg/L H_2O_2	0.3mg/L Fe^{3+} 5mg/L H_2O_2
0.3mg/L Fe^{3+} 10mg/L H_2O_2	0.3mg/L Fe^{3+} 10mg/L H_2O_2

Appendix D: ICP-OES and 1,10 Phenanthroline Iron Concentrations

A series of time-based dark and irradiated Fenton experiments for LCT and well water were carried out to determine 1) if iron was absorbing to the quartz vessel, 2) the fraction of soluble an insoluble ferric and ferrous iron and 3) if 1,10 Phenanthroline and OES results were in agreement. With the exception of test 3, colloidal iron formed instantly when stock was added to the sample. Notes are listed at the bottom of this Appendix.

Ferrous , LCT

	Test 1:	Ferrous stock, 15mg added to 200mL Milli-Q water	
	Time (mins)	Method	Iron (mg/L)
Total Iron	0	1, 10 phenanthroline	14.9
Ferrous	0	1, 10 phenanthroline	7.75
Ferrous acidified	0	1, 10 phenanthroline	13.75
Total Iron	0	ICP-OES	15.25
Total Iron 0.2um Filtered	0	ICP-OES	15.08
Stock after 5 hrs	300	ICP-OES	14.4
	Test 2:	Dark, 0.3 mg/L	
Total Iron	0	1, 10 phenanthroline	0.29
Ferrous iron	0	1, 10 phenanthroline	0.03
Ferrous iron acidified	0	1, 10 phenanthroline	0.04
Total iron	0	ICP-OES	0.3045
Total iron 0.2um filtered	0	ICP-OES	0.219
Total iron, 10 mg/L H_2O_2	0	ICP-OES	0.31
Total iron, 0.2um filtered, 10 mg/L H_2O_2	0	ICP-OES	DL
Total iron, 10 mg/L H_2O_2	18	ICP-OES	0.311
Total iron, 0.2um filtered, 10 mg/L H_2O_2	18	ICP-OES	DL
Total iron [1]	300	ICP-OES	0.297
Total iron 0.2um filtered	300	ICP-OES	DL
	Test 3:	Dark, 0.1 mg/L	
Total iron	0	1, 10 phenanthroline	0.11
Total iron	0	ICP-OES	0.124
Total iron, 0.2um filtered	0	ICP-OES	0.089
Total iron, 10 mg/L H_2O_2	18	ICP-OES	0.096
Total iron, 0.2um filtered, 10 mg/L H_2O_2	18	ICP-OES	DL
	Test 4:	UV, 0.3 mg/L	
Total iron	18	ICP-OES	0.322
Total iron 0.2um filtered	18	ICP-OES	DL
Total iron, 10 mg/L H_2O_2	18	ICP-OES	0.289
Total iron, 0.2um filtered, 10 mg/L H_2O_2	18	ICP-OES	DL
	Test 5:	UV, 0.1 mg/L	
Total iron	18	ICP-OES	0.101
Total iron 0.2um filtered	18	ICP-OES	DL
Total iron, 10 mg/L H_2O_2	18	ICP-OES	0.1

	Time (mins)	Method	Iron (mg/L)
Total iron, 0.2um filtered, 10 mg/L H_2O_2	18	ICP-OES	DL

Ferrous, Well

Test 6:	**Dark, 0.3 mg/L**		
	Time (mins)	Method	Iron (mg/L)
Total Iron	0	1, 10 phenanthroline	0.29
Ferrous iron	0	1, 10 phenanthroline	0.02
Ferrous iron acidified	0	1, 10 phenanthroline	0.04
Total iron	0	ICP-OES	0.3021
Total iron 0.2um filtered	0	ICP-OES	DL
Total iron, 10 mg/L H_2O_2	0	ICP-OES	0.3022
Total iron, 0.2um filtered, 10 mg/L H_2O_2	0	ICP-OES	DL
Total iron, 10 mg/L H_2O_2	18	ICP-OES	0.3
Total iron, 0.2um filtered, 10 mg/L H_2O_2	18	ICP-OES	DL
Total iron	300	ICP-OES	0.297
Total iron 0.2um filtered	300	ICP-OES	DL
Test 7:	**Dark, 0.1 mg/L**		
Total iron	0	1, 10 phenanthroline	0.1
Total iron	0	ICP-OES	0.121
Total iron, 0.2um filtered	0	ICP-OES	0.098
Total iron, 10 mg/L H_2O_2	18	ICP-OES	0.096
Total iron, 0.2um filtered, 10 mg/L H_2O_2	18	ICP-OES	DL
Test 8:	**UV, 0.3 mg/L**		
Total iron	18	ICP-OES	0.302
Total iron 0.2um filtered	18	ICP-OES	DL
Total iron, 10 mg/L H_2O_2	18	ICP-OES	0.209
Total iron, 0.2um filtered, 10 mg/L H_2O_2	18	ICP-OES	DL
Test 9:	**UV, 0.1 mg/L Ferrous**		
Total iron	18	ICP-OES	0.111
Total iron 0.2um filtered	18	ICP-OES	DL
Total iron, 10 mg/L H_2O_2	18	ICP-OES	0.082
Total iron, 0.2um filtered, 10 mg/L H_2O_2	18	ICP-OES	DL

Ferric, LCT

	Time (mins)	Method	Iron (mg/L)
Test 10:	**Ferric stock, 11mg added to 200mL Milli-Q water**		
Total Iron	0	1, 10 phenanthroline	10.6
Ferrous	0	1, 10 phenanthroline	0.25
Ferrous acidified	0	1, 10 phenanthroline	0.25
Total Iron	0	ICP-OES	10.881
Total Iron 0.2um Filtered	0	ICP-OES	10.749
Stock after 4 hrs	300	ICP-OES	10.62
Test 11:	**Dark, 0.3 mg/L**		
Total Iron	0	1, 10 phenanthroline	0.3
Ferrous iron	0	1, 10 phenanthroline	DL
Ferrous iron acidified	0	1, 10 phenanthroline	DL
Total iron	0	ICP-OES	0.309
Total iron 0.2um filtered	0	ICP-OES	DL
Total iron, 10 mg/L H_2O_2	0	ICP-OES	0.309
Total iron, 0.2um filtered, 10 mg/L H_2O_2	0	ICP-OES	0.014
Total iron, 10 mg/L H_2O_2	18	ICP-OES	0.294
Total iron, 0.2um filtered, 10 mg/L H_2O_2	18	ICP-OES	0.048
Total iron	300	ICP-OES	0.307
Total iron 0.2um filtered	300	ICP-OES	DL
Test 12:	**Dark, 0.1 mg/L**		
Total iron	0	1, 10 phenanthroline	0.1
Total iron	0	ICP-OES	0.101
Total iron, 0.2um filtered	0	ICP-OES	DL
Total iron, 10 mg/L H_2O_2	18	ICP-OES	0.1
Total iron, 0.2um filtered, 10 mg/L H_2O_2	18	ICP-OES	DL
Test 13:	**UV, 0.3 mg/L**		
Total iron	18	ICP-OES	0.289
Total iron 0.2um filtered	18	ICP-OES	DL
Total iron, 10 mg/L H_2O_2	18	ICP-OES	0.289
Total iron, 0.2um filtered, 10 mg/L H_2O_2	18	ICP-OES	DL
Test 14:	**UV, 0.1 mg/L**		
Total iron	18	ICP-OES	0.103
Total iron 0.2um filtered	18	ICP-OES	DL
Total iron, 10 mg/L H_2O_2	18	ICP-OES	0.083
Total iron, 0.2um filtered, 10 mg/L H_2O_2	18	ICP-OES	DL

Ferric, Well

Test 15: Dark, 0.3 mg/L

	Time (mins)	Method	Iron (mg/L)
Total Iron	0	1, 10 phenanthroline	0.3
Ferrous iron	0	1, 10 phenanthroline	DL
Ferrous iron acidified	0	1, 10 phenanthroline	DL
Total iron	0	ICP-OES	0.303
Total iron 0.2um filtered	0	ICP-OES	DL
Total iron, 10 mg/L H_2O_2	0	ICP-OES	0.301
Total iron, 0.2um filtered, 10 mg/L H_2O_2	0	ICP-OES	DL
Total iron, 10 mg/L H_2O_2	18	ICP-OES	0.280
Total iron, 0.2um filtered, 10 mg/L H_2O_2	18	ICP-OES	DL
Total iron	300	ICP-OES	0.307
Total iron 0.2um filtered	300	ICP-OES	DL

Test 16: Dark, 0.1 mg/L

	Time (mins)	Method	Iron (mg/L)
Total iron	0	1, 10 phenanthroline	0.1
Total iron	0	ICP-OES	0.121
Total iron, 0.2um filtered	0	ICP-OES	DL
Total iron, 10 mg/L H_2O_2	18	ICP-OES	0.1
Total iron, 0.2um filtered, 10 mg/L H_2O_2	18	ICP-OES	DL

Test 17: UV, 0.3 mg/L

	Time (mins)	Method	Iron (mg/L)
Total iron	18	ICP-OES	0.303
Total iron 0.2um filtered	18	ICP-OES	DL
Total iron, 10 mg/L H_2O_2	18	ICP-OES	0.210
Total iron, 0.2um filtered, 10 mg/L H_2O_2	18	ICP-OES	DL

Test 18: UV, 0.1 mg/L Ferrous

	Time (mins)	Method	Iron (mg/L)
Total iron	18	ICP-OES	0.121
Total iron 0.2um filtered	18	ICP-OES	DL
Total iron, 10 mg/L H_2O_2	18	ICP-OES	0.07
Total iron, 0.2um filtered, 10 mg/L H_2O_2	18	ICP-OES	DL

Notes:

(1) Same ferrous and ferric iron stock solution used for all experiments - tests performed within a 5-hour time frame. Stock re-tested after experiments were completed (300 mins).

(2) ICP-OES detection limit 0.012 mg/L

(3) HACH 1, 10 phenanthroline detection limit is 0.2 mg/L.

Appendix E: Observed Temperature and pH Changes

The following experiments were conducted in well water to monitor pH and temperature changes during dark and irradiated experiments. Exposure times were 18 minutes to reflect maximum fluence rates (~800 mJ/cm^2).

Scenario	H$_2$O$_2$ (mg/L)	Initial Temp. (°C)	Final Temp. (°C)	% Difference in Temp.	Initial pH	Final pH
Dark	0	18	19	5%	8.20	8.21
Dark	10	18	19	5%	8.22	8.19
Dark, 0.1 mg/L Fe2+	0	18	19	5%	8.15	8.20
Dark, 0.3 mg/L Fe2+	0	18	19	5%	8.15	8.19
Dark, 0.1 mg/L Fe2+	10	19	21	10%	8.15	8.20
Dark, 0.3 mg/L Fe2+	10	19	21	10%	8.15	8.15
Dark, 0.3 mg/L Fe3+	0	17	18	6%	8.31	8.10
Dark, 0.1 mg/L Fe3+	0	17	18	6%	8.31	8.20
Dark, 0.3 mg/L Fe3+	10	20	22	9%	8.11	8.20
Dark, 0.1 mg/L Fe3+	10	20	22	9%	8.11	8.10
UV	0	12	16	25%	8.18	8.12
UV	10	12	16	25%	8.18	8.13
UV, 0.3 mg/L Fe 2+	0	14	18	28%	8.18	8.16
UV, 0.1 mg/L Fe 2+	0	15	17	29%	8.18	8.21
UV, 0.3 mg/L Fe 2+	10	14	18	28%	8.18	8.29
UV, 0.1 mg/L Fe 2+	10	13	17	29%	8.18	8.21
UV, 0.3 mg/L Fe3+	0	11	15	33%	8.15	8.19
UV, 0.1 mg/L Fe3+	0	13	16	25%	8.15	8.22
UV, 0.3 mg/L Fe3+	10	11	15	33%	8.15	8.18
UV, 0.1 mg/L Fe3+	10	12	16	25%	8.15	8.22

Appendix F: HPLC control experiments

To ensure chemicals were not complexing with iron before or after UV irradiation, peak HPLC areas were examined pre and post filtration and acidification. Experiments were performed in well water.

Scenario	Filter	Iron Addition (mg/L Fe^{2+})	Average Peak Area
pCBA 0.5 mg/L	--	--	244.3
	0.45 um	--	226
	--	0.3	229.5
	0.45 um	0.3	215.4
Not acidified	--	0.3	230.1
Acidified	0.45 um	0.3	214.4
800 mJ/cm^2 exposure	--	0.3	11.8
Acidified	0.45 um	0.3	11.6
NDMA 0.5 mg/L	--	--	301.1
	0.45 um	--	304.5
	--	0.3	301.75
	0.45 um	0.3	299.5
Not acidified	--	0.3	301
Acidified	0.45 um	0.3	300.8
800 mJ/cm^2 exposure	--	0.3	23.65
Acidified	0.45 um	0.3	22.9
CBZ 0.5 mg/L	--	--	275.15
	0.2 um	--	274.65
	--	0.3	267.1
	0.2 um	0.3	268.75
Not acidified	--	0.3	256
Acidified	0.2 um	0.3	256.45
800 mJ/cm^2 exposure	--	0.3	93.6
Acidified	0.2 um	0.3	92.6

Appendix G: Dark and UV-Irradiated Chemical Control Tests

The following time-based control tests were conducted in LCT and well water to determine if dark-Fenton reactions contributed to chemical degradation. UV-only tests are presented for pCBA and CBZ to illustrate the minimal contribution of UV photolysis on chemical removal.
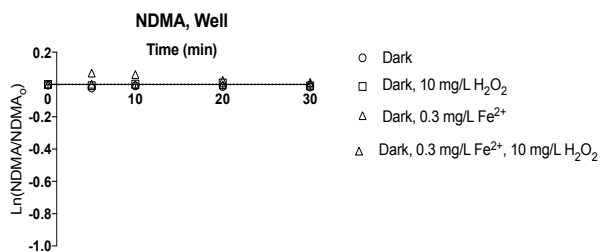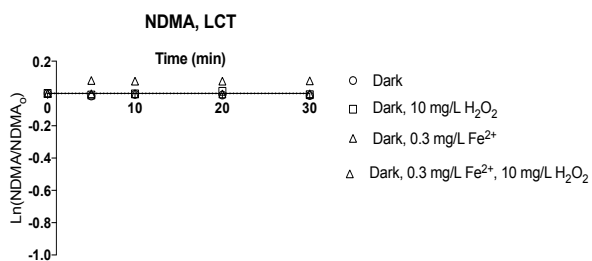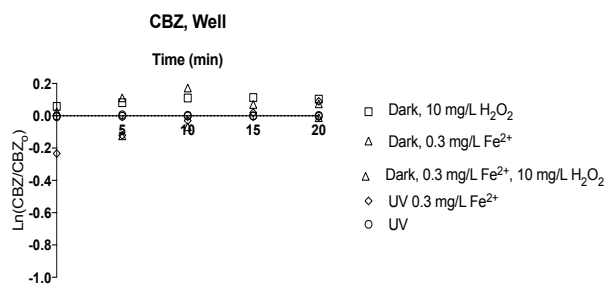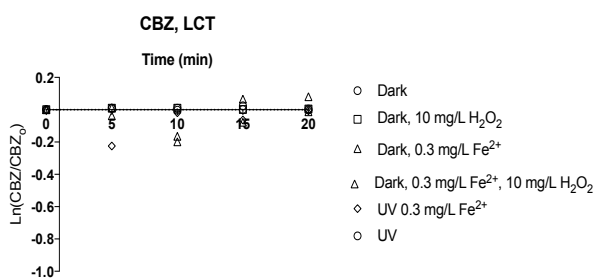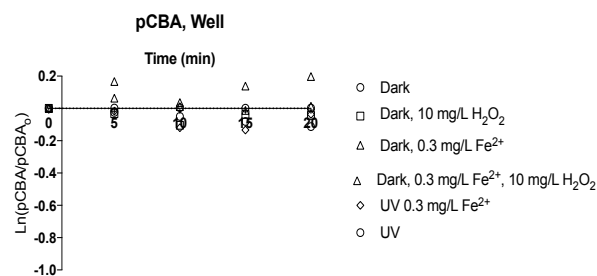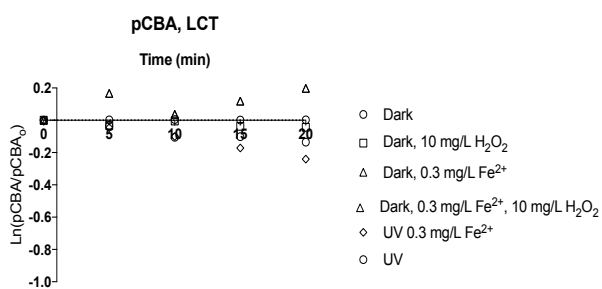
Appendix H: Determination of Hydroxyl Radical Steady-State Concentrations for pCBA and CBZ

The steady-state HO˙ concentrations for pCBA and CBZ were determined by using the following relationship:

$$\ln\frac{[C]}{[C]_o} = \frac{-k_{OH,C}[\bullet OH]}{E_o} \times F \qquad (1)$$

where E_o is the average fluence rate (mW/cm^2), which considers the incidence irradiance (radiometer reading), petri factor, water factor, divergence factor, and reflection factor, F is the fluence (mJ/cm^2) and $k_{HO,C}$ (M^{-1}s^{-1}) is a time-based reaction rate constant between chemical, C, and hydroxyl radicals.

$\dfrac{k_{OH,C}[HO]_{ss}}{E_o}$ is the slope of the plot of ln([pCBA]/[pCBA]$_0$) *vs F*. As an example, the slope of Figure 14 is -4.2447 x 10^3 cm^2/mJ. Using the slope [HO˙] can then be calculated as:

$$[\bullet OH] = \frac{slope * E_o}{k_{OH,C}} \qquad (2)$$
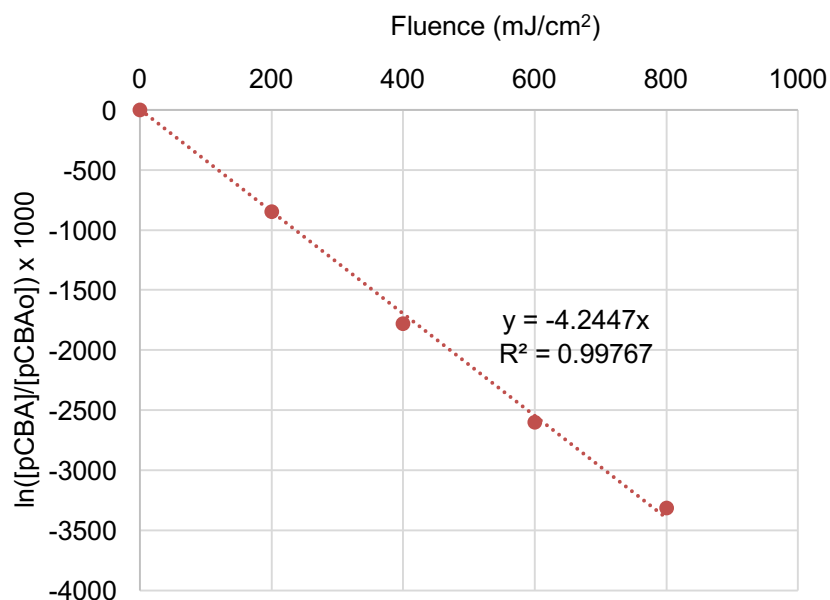
Figure 14. Example showing the slope used to determine steady-state HO˙ concentrations by plotting the natural log of the ratio of chemical concentration at a given fluence over the initial chemical concentration with respect to UV fluence.

Known k_{OH} values of 5×10^9 and 6.4×10^9 $M^{-1}s^{-1}$ for pCBA and CBZ, respectively, were used. HO˙ steady state concentrations are presented in Table 8.

Table 8. Average hydroxyl radical steady state concentrations determined for LCT and well water.

Chemical	Experiment	LCT Average [OH] (M)	Well Average [OH] (M)
pCBA	5mg/L H_2O_2	5.872E-13	1.095E-13
	0.1mg/L Fe^{2+} 5mg/L H_2O_2	6.008E-13	1.327E-13
	0.3mg/L Fe^{2+} 5mg/L H_2O_2	5.945E-13	1.425E-13
	0.1mg/L Fe^{3+} 5mg/L H_2O_2	5.722E-13	1.292E-13
	0.3mg/L Fe^{3+} 5mg/L H_2O_2	5.995E-13	1.336E-13
	10mg/L H_2O_2	8.410E-13	2.145E-13
	0.1mg/L Fe^{2+} 10mg/L H_2O_2	9.161E-13	2.609E-13
	0.3mg/L Fe^{2+} 10mg/L H_2O_2	9.825E-13	2.651E-13
	0.1mg/L Fe^{3+} 10mg/L H_2O_2	9.213E-13	2.783E-13
	0.3mg/L Fe^{3+} 10mg/L H_2O_2	8.883E-13	2.827E-13
CBZ	5mg/L H_2O_2	3.012E-13	1.237E-13
	0.1mg/L Fe^{2+} 5mg/L H_2O_2	3.266E-13	1.537E-13
	0.3mg/L Fe^{2+} 5mg/L H_2O_2	2.961E-13	1.751E-13
	0.1mg/L Fe^{3+} 5mg/L H_2O_2	3.709E-13	1.220E-13
	0.3mg/L Fe^{3+} 5mg/L H_2O_2	2.811E-13	1.206E-13
	10mg/L H_2O_2	5.936E-13	2.509E-13
	0.1mg/L Fe^{2+} 10mg/L H_2O_2	4.873E-13	2.673E-13
	0.3mg/L Fe^{2+} 10mg/L H_2O_2	6.129E-13	2.562E-13
	0.1mg/L Fe^{3+} 10mg/L H_2O_2	6.113E-13	2.298E-13
	0.3mg/L Fe^{3+} 10mg/L H_2O_2	5.259E-13	2.306E-13

Appendix I: Degradation Rate Constants

Fluence-based degradation rate constants represent the slope of the plot illustrated in Figure 14.

Chemical	Experiment	LCT Average k'_{obs} (cm^2/mJ)	Variance (cm^2/mJ)	Confidence*
pCBA	UV	1.506E-04	3.100E-10	
	5mg/L H_2O_2	3.087E-03	4.220E-11	
	0.1mg/L Fe^{2+} 5mg/L H_2O_2	3.155E-03	4.427E-09	--
	0.3mg/L Fe^{2+} 5mg/L H_2O_2	3.123E-03	8.487E-10	--
	0.1mg/L Fe^{3+} 5mg/L H_2O_2	3.012E-03	5.346E-09	95%
	0.3mg/L Fe^{3+} 5mg/L H_2O_2	3.148E-03	1.479E-10	--
	10mg/L H_2O_2	4.356E-03	2.460E-08	
	0.1mg/L Fe^{2+} 10mg/L H_2O_2	4.731E-03	7.321E-09	95%
	0.3mg/L Fe^{2+} 10mg/L H_2O_2	5.063E-03	1.836E-08	95%
	0.1mg/L Fe^{3+} 10mg/L H_2O_2	4.757E-03	1.804E-07	--
	0.3mg/L Fe^{3+} 10mg/L H_2O_2	4.592E-03	9.531E-08	--
CBZ	UV	2.510E-05	2.832E-10	
	5mg/L H_2O_2	2.063E-03	4.250E-09	
	0.1mg/L Fe^{2+} 5mg/L H_2O_2	2.225E-03	3.616E-08	--
	0.3mg/L Fe^{2+} 5mg/L H_2O_2	2.030E-03	2.540E-08	--
	0.1mg/L Fe^{3+} 5mg/L H_2O_2	2.509E-03	2.294E-08	95%
	0.3mg/L Fe^{3+} 5mg/L H_2O_2	1.934E-03	1.344E-07	--
	10mg/L H_2O_2	3.934E-03	2.509E-10	
	0.1mg/L Fe^{2+} 10mg/L H_2O_2	3.254E-03	3.115E-08	(-95%)
	0.3mg/L Fe^{2+} 10mg/L H_2O_2	4.058E-03	2.745E-09	95%
	0.1mg/L Fe^{3+} 10mg/L H_2O_2	4.048E-03	3.696E-08	--
	0.3mg/L Fe^{3+} 10mg/L H_2O_2	3.501E-03	7.092E-09	(-95%)
NDMA	UV	1.763E-03	1.895E-08	
	5mg/L H_2O_2	1.985E-03	6.613E-09	
	0.1mg/L Fe^{2+} 5mg/L H_2O_2	2.043E-03	1.306E-09	--
	0.3mg/L Fe^{2+} 5mg/L H_2O_2	2.474E-03	2.442E-10	95%
	0.1mg/L Fe^{3+} 5mg/L H_2O_2	2.303E-03	2.694E-09	95%
	0.3mg/L Fe^{3+} 5mg/L H_2O_2	2.426E-03	1.513E-09	95%
	10mg/L H_2O_2	2.501E-03	9.248E-11	
	0.1mg/L Fe^{2+} 10mg/L H_2O_2	2.780E-03	5.030E-09	95%
	0.3mg/L Fe^{2+} 10mg/L H_2O_2	3.027E-03	5.274E-10	95%
	0.1mg/L Fe^{3+} 10mg/L H_2O_2	2.572E-03	7.321E-09	--
	0.3mg/L Fe^{3+} 10mg/L H_2O_2	2.711E-03	2.139E-09	95%

		Well		
Chemical	Experiment	Average k'_{obs} (cm^2/mJ)	Variance (cm^2/mJ)	Confidence*
pCBA	UV	1.351E-04	7.411E-10	
	5mg/L H_2O_2	6.827E-04	4.381E-10	
	0.1mg/L Fe^{2+} 5mg/L H_2O_2	7.983E-04	9.946E-10	95%
	0.3mg/L Fe^{2+} 5mg/L H_2O_2	8.475E-04	5.832E-11	95%
	0.1mg/L Fe^{3+} 5mg/L H_2O_2	7.809E-04	1.496E-10	95%
	0.3mg/L Fe^{3+} 5mg/L H_2O_2	8.029E-04	7.442E-11	95%
	10mg/L H_2O_2	1.208E-03	4.090E-10	
	0.1mg/L Fe^{2+} 10mg/L H_2O_2	1.440E-03	8.978E-11	95%
	0.3mg/L Fe^{2+} 10mg/L H_2O_2	1.460E-03	1.232E-10	95%
	0.1mg/L Fe^{3+} 10mg/L H_2O_2	1.527E-03	7.663E-09	95%
	0.3mg/L Fe^{3+} 10mg/L H_2O_2	1.549E-03	3.432E-10	95%
CBZ	UV	1.285E-05	1.711E-12	
	5mg/L H_2O_2	8.046E-04	7.411E-12	
	0.1mg/L Fe^{2+} 5mg/L H_2O_2	9.967E-04	2.928E-10	95%
	0.3mg/L Fe^{2+} 5mg/L H_2O_2	1.134E-03	5.724E-11	95%
	0.1mg/L Fe^{3+} 5mg/L H_2O_2	7.939E-04	3.289E-11	--
	0.3mg/L Fe^{3+} 5mg/L H_2O_2	7.847E-04	2.311E-10	--
	10mg/L H_2O_2	1.618E-03	1.510E-09	
	0.1mg/L Fe^{2+} 10mg/L H_2O_2	1.723E-03	4.127E-09	--
	0.3mg/L Fe^{2+} 10mg/L H_2O_2	1.653E-03	2.311E-10	--
	0.1mg/L Fe^{3+} 10mg/L H_2O_2	1.483E-03	1.326E-11	(-95%)
	0.3mg/L Fe^{3+} 10mg/L H_2O_2	1.489E-03	2.798E-09	--
NDMA	UV	1.853E-03	5.447E-09	
	5mg/L H_2O_2	2.414E-03	1.815E-08	
	0.1mg/L Fe^{2+} 5mg/L H_2O_2	3.082E-03	1.066E-10	95%
	0.3mg/L Fe^{2+} 5mg/L H_2O_2	3.082E-03	1.066E-10	95%
	0.1mg/L Fe^{3+} 5mg/L H_2O_2	2.990E-03	7.220E-10	95%
	0.3mg/L Fe^{3+} 5mg/L H_2O_2	3.163E-03	1.620E-10	95%
	10mg/L H_2O_2	2.765E-03	4.140E-09	
	0.1mg/L Fe^{2+} 10mg/L H_2O_2	3.192E-03	8.939E-09	95%
	0.3mg/L Fe^{2+} 10mg/L H_2O_2	3.361E-03	3.518E-08	95%
	0.1mg/L Fe^{3+} 10mg/L H_2O_2	3.276E-03	2.681E-08	95%
	0.3mg/L Fe^{3+} 10mg/L H_2O_2	3.312E-03	1.644E-08	95%

*A two-tailed t-test was used to determine a confidence interval of 95%. Negative results, shown in parentheses, indicate iron inhibited chemical reduction.

Appendix J: Model Inputs and Methods

Modeling of pCBA, CBZ and NDMA UV-AOP follows methods presented by Rosenfeldt, Sharpless and Linden (Rosenfeldt and Linden, 2007, Sharpless and Linden, 2003). Model inputs are presented in Table 9 and are specific to 254nm.

Table 9. Model inputs.

Chemical	$k_{OH \cdot}$ M^{-1}s^{-1} (a) M^{-1}s^{-1}	$\Phi254$ (10^{-2}) (b) mol/Einstein	ε_{254} (10^3) (c) M^{-1}cm^{-1}
pCBA	5.00E+09	1.30	2.37
CBZ	6.40E+09	0.06	6.07
NDMA	3.30E+08	0.30	1.65
H$_2$O$_2$	2.70E+07	1	19
TOC (L/mg s^{-1})	2.50E+04	--	--
HCO$_3^-$	8.50E+06	--	--
CO$_3^{-2}$	3.90E+08	--	--

(a)-(c) Buxton et al., 1988; Wols and Hofman-Caris, 2012; Sharpless and Linden, 2003.

The model assumes steady-state conditions and considers the impact direct and indirect photolysis have on the chemicals of interest, *C*, under varied H$_2$O$_2$ concentrations and water quality conditions. An example is provided below using pCBA + 5 mg/L H$_2$O$_2$ with and without Fe(II) addition. All model inputs are provided in Table 10 and plotted results are shown in Figure 15

Table 10. Model inputs for pCBA + 5 mg/L H$_2$O$_2$ with and without 0.3 mg/L Fe^{2+} in well water.

Energy of 1 Es @254 nm wavelength

Na	6.02E+23	mol^{-1}
h	6.62E-34	J s
c	3.00E+08	m s^{-1}
l	2.54E-07	m
U	4.71E+05	J Es^{-1}

Scavenging Information

k(OH,DOC/TOC)	2.50E+04	L/mg s^{-1}
k(OH,HCO$_3^-$)	8.50E+06	M^{-1} s^{-1}
k(OH,CO$_3^{-2}$)	3.90E+08	M^{-1} s^{-1}
k(OH,NO$_2^-$)	1.30E+09	M^{-1} s^{-1}
k(OH,H$_2$O$_2$)	2.70E+07	M^{-1} s^{-1}
k(OH,M)	5.00E+09	M^{-1} s^{-1}

UV Data:	0Fe5+H2O2UVW	0.3Fe2+5H2O2UVW	
Incident Irradiance (E_o)	1.013	1.014	mW cm^{-2}
Sample Depth (b)	2.27	2.27	cm
UV abs$_{254}$	2.06E-02	3.99E-02	cm^{-1}
A=2.303*abs*b	0.10756	0.20840	(base e)
Average Irradiance, total vol.	0.806	0.813	mW cm^{-2}
Average Irradiance	0.960	0.939	mW cm^{-2}
Water Quality Data:			
pH	7.82	7.82	
TOC	1.150	1.150	mg L^{-1}
Nitrite	0.000	0.000	ppm
Nitrite	0.00E+00	0.00E+00	M
alkalinity as CaCO$_3$	285	285	mg CaCO$_3$ L^{-1}
alkalinity as CaCO$_3$	0.00285	0.00285	M
alkalinity as HCO3-	347.7	347.7	mg HCO$_3$ L^{-1}
alkalinity as HCO3-	0.0057	0.0057	M
Scavenging Information			
k(OH,DOC/TOC)[S]	2.88E+04	2.88E+04	s^{-1}
k(OH,HCO$_3^-$)[S]	2.41E+04	2.41E+04	s^{-1}
k(OH,CO$_3^{-2}$)[S]	3.66E+03	3.66E+03	s^{-1}
k(OH,NO$_2^-$)[S]	0.00E+00	0.00E+00	s^{-1}
k(OH,H$_2$O$_2$)[S]	3.91E+03	3.91E+03	s^{-1}
k(OH,M)[S]	1.60E+04	1.59E+04	s^{-1}
Total k*[S]=	6.04E+04	6.04E+04	s^{-1}
Initial Oxidant Dose:			
H$_2$O$_{2,i}$	4.93	4.93	ppm
[H$_2$O$_2$]$_i$	1.45E-04	1.45E-04	M
QY$_{H2O2}$	1	1	mol Es-1
e$_{H2O2}$	19	19	M^{-1} cm^{-1}
Pollutant "M" Information			
[M]i	0.500298571	0.497934121	(mg/L)
[M]i	3.19E-06	3.18E-06	M
kOH,M	5.00E+09	5.00E+09	M-1s-1
QY$_M$	0.013	0.013	mol Es-1
Abs M @ 254nm	2.06E-02	2.06E-02	
l (cell path length)	1	1	cm
e$_M$	2370.0	2370.0	M-1 cm-1
OH Radical Formation Calculations			
Incident Photon Irradiance	2.15E-06	2.21E-06	mEs cm^{-2} s^{-1}
Average Photon Irradiance	2.04E-06	1.99E-06	mEs cm^{-2} s^{-1}

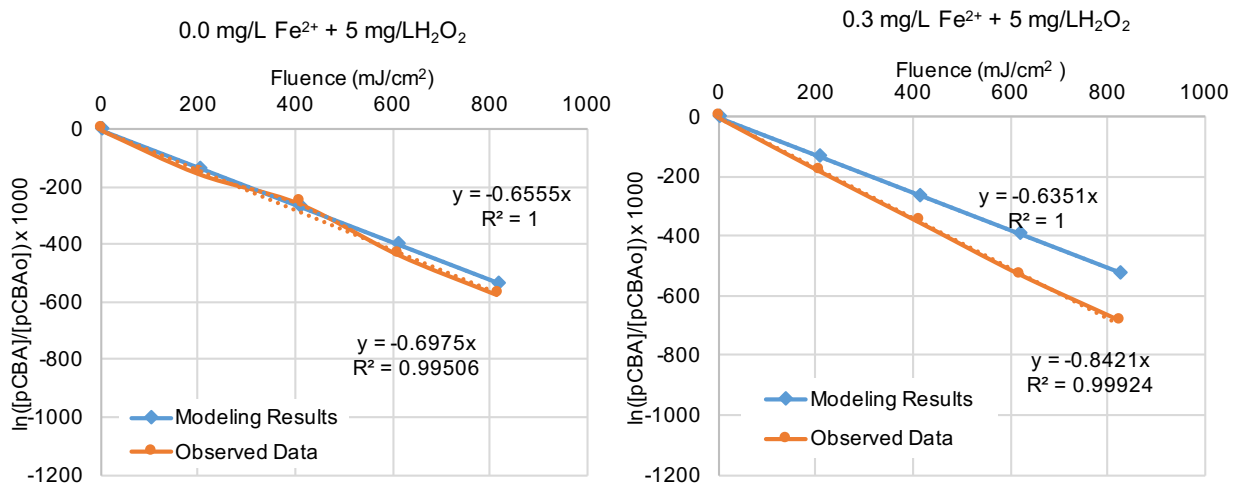|		
OH formation	5.62E-09	5.49E-09	M s^{-1}
Indirect Photolysis, OH Radical Oxidation Rate Calculations		
Modeled [OH]$_{ss}$	9.31E-14	9.10E-14	M
k'(OH)	4.65E-04	4.55E-04	s^{-1}
k'(OH)I	5.77E-04	5.59E-04	cm^2 mJ^{-1}
Direct Photolysis Rate Calculations		
Average Photon Irradiance	2.04E-06	1.99E-06	mEs cm^{-2} s^{-1}
k'(Direct)	6.29E-05	6.15E-05	s^{-1}
k'(Direct)$_D$	7.80E-05	7.56E-05	cm^2 mJ^{-1}
k'(Total)$_D$ = k'(OH)$_D$ + k'(Direct)$_D$	6.56E-04	**6.35E-04**	**cm^2 mJ^{-1}**

Figure 15. A comparison between modeled and experimental results for pCBA + 5 mg/L H$_2$O$_2$ with and without 0.3 mg/L Fe^{2+} in well water. Corresponding input values are provided in Table 10.

Appendix K: Discussion on NDMA Modeled Results

Modeled and predicted NDMA results were off by approximate factors of 1.4 and 1.6 for LCT and well water, respectively (example shown in Figure 16). Since pCBA and CBZ modeled results for control tests (UV, UV + 5 mg/L H_2O_2 and UV + 10 mg/L H_2O_2) align well will experimental results and for reasons outlined below, it has been initially assumed an error occurred within the model rather than experimentally. An overview of what was done and what could be done to determine where the error is occurring is provided below.
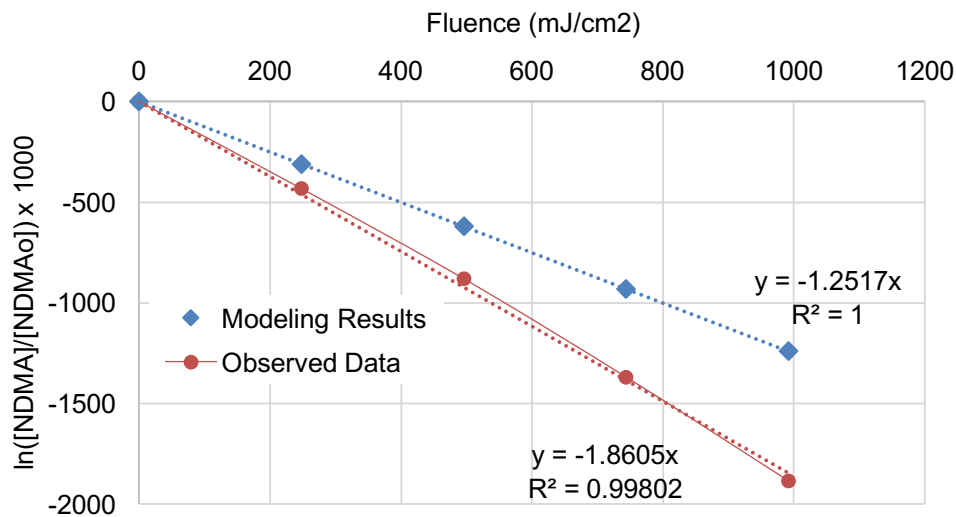

Figure 16. A comparison of NDMA UV-only modeled and experimental results.

Model tests:

A range of values for quantum yield, molar absorption coefficients, and second order hydroxyl radical reactions, found in published literature, were inputted into the model with little change in modeled results (Sharpless and Linden, 2003; Wols and Hofman-Caris, 2012).

Experimental tests:

Control experiments were conducted in quadruplicate over a 6-month time period. Two of these experiments used varied sample volume, petri dish size, and distance from the UV lamps to the surface of the water. When comparing the degradation rates between different experimental setups, UV-only removal rates in LCT water were within ±0.20 (x 10^{-3}) cm^2/mJ which would not account for the 0.60 (x 10^{-3}) cm^2/mJ difference between the model and experimental results. (This was also shown for time-based rate constants.)

Additional experimental factors that could potentially be impacting experimental results include the radiometer reading (incident intensity), increased temperature during UV exposure, and inadequate mixing. All radiometer readings were within ± 0.14 mW/cm^2 of one another over a year and a half long testing period, and within this timeframe the radiometer was re-calibrated. Sharpless et al. observed NDMA degradation by UV photolysis increased by 10% and 20% when the temperature increased from 3°C to 13°C and 13°C to 25%, respectively. For the experiments conducted only a 4°C (12°C to 16°C) increase in temperature occurred over maximum exposure (~17 minutes) and the model and observed control (UV, UV + 5 mg/L H$_2$O$_2$ and UV + 10 mg/L H$_2$O$_2$) results were off by approximately 36% in LCT water and 46% in the well water. Samples were continuously stirred during irradiation and swirled by hand prior to sampling.

Additional experiments and modeling tests:

- Using a new NDMA stock solution, the experiments could be carried out in a jacketed quartz vessel to control temperature.
- An actinometer could be used to verify radiometer-determined incident irradiance values.
- The model could be re-constructed for factors influencing direct photolysis.

Appendix L: Proposed NDMA Kinetic Experiment

A kinetics experiment using isopropyl alcohol (IPA) (or other chemical known not to react with ferryl) as a competitor and NDMA as a probe compound could be conducted to determine the influence of oxidative species other than $\cdot OH$ on NDMA removal. Methods outlined below followed those presented by Sun et al. (Sun et al., 2015). Equation 1 can be used to determine the increase in the initial degradation rate constant with increasing concentrations of the oxidant competitor, IPA.

$$R_{NDMA,IPA} = R_{NDMAo} \frac{k_{NDMA}[NDMA]}{k_{IPA}[IPA] + k_{NDMA}[NDMA]} \qquad (1)$$

where [NDMA] and [IPA] are the concentrations of the probe and competitor, respectively. R_{NDMAo} is the initial pseudo-first-order reaction rate constant in the absence of IPA addition and $R_{NDMA, IPA}$ is the pseudo-first-order reaction rate constant with different concentrations of competitor added. k_{IPA} and k_{NDMA} are the second order reaction rate constants with the oxidizing specie. Equation 1 can then be rearranged to yield equation 2.

$$\frac{R_{NDMAo}}{R_{NDMA,IPA}} = 1 + \left(\frac{k_{IPA}}{k_{NDMA}}\right)\left(\frac{[IPA]}{[probe]}\right) \qquad (2)$$

The ratios of the rate constants, $R_{NDMAo}/ R_{NDMA, IPA}$, can be plotted with respect to *[IPA]/[NDMA]* to determine the slope of the second order reaction rate constants, k_{IPA}/k_{NDMA}. The slope can then be compared to literature values and deviations can be observed in photo-Fenton systems.